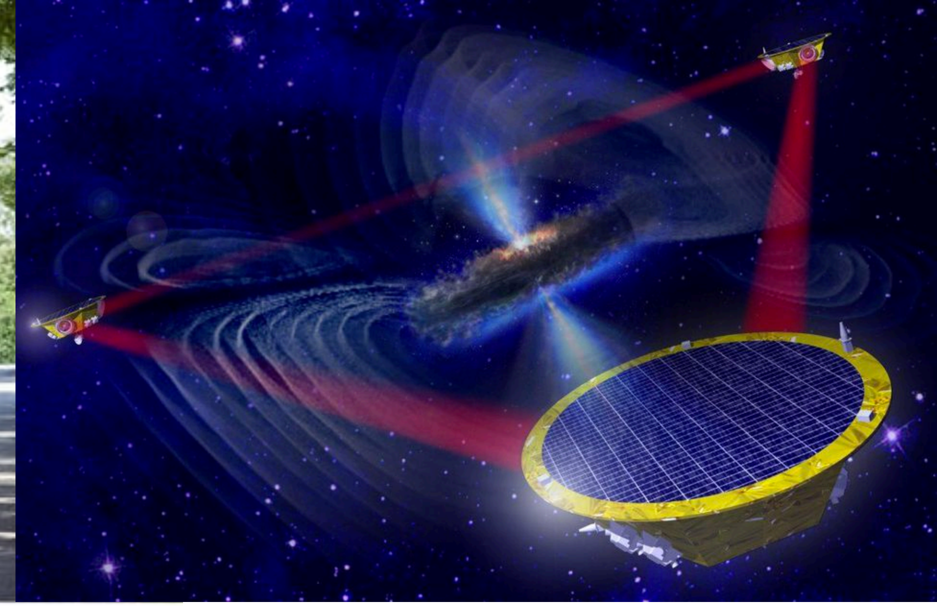

Primordial Turbulent Sources for Gravitational Waves

Physics
Carnegie Mellon University

Tina Kahniashvili

September 18, 2019

collaboration

- Axel Brandenburg (NORDITA, Sweden)
- Alexey Boyarsky (Leiden University, Netherland)
- Leonardo Campanelli (Bari University, Italy)
- Ruth Durrer (Geneva University, Swiss)
- Jurg Frohlich (ETH-Zurich, Swiss)
- Giga Gogoberidze (IliaUni, Georgia)
- Nathan Kleeorin (Ben-Gurion University, Israel)
- Arthur Kosowsky (University of Pittsburgh, USA)
- Sayan Mandal (CMU, USA)
- Andrii Neronov (APC, France)
- Bharat Ratra (KSU, USA)
- Igor Rogachevskii (Ben-Gurion University, Israel)
- Oleg Ruchayskirsky (Niels Bohr Institute, Denmark)
- Alberto Roper Pol (CU-Boulder, USA)
- Jennifer Schober (EPFL-Lausanne, Swiss)
- Alexander Tevzadze (TSU, Georgia)
- Tanmay Vachaspati (ASU, USA)
- Winston Yin (CMU, USA)

outline

- Overview
- Primordial gravitational waves from primordial turbulence
- Primordial MHD turbulence
- Numerical simulations
- LISA and primordial gravitational waves

gravitational waves astronomy

- **Advantage**

Connection with High Energy Physics – the best laboratory to test the energy scales EVEN near the Planck scale

- **Disadvantage**

Direct detection is complicated

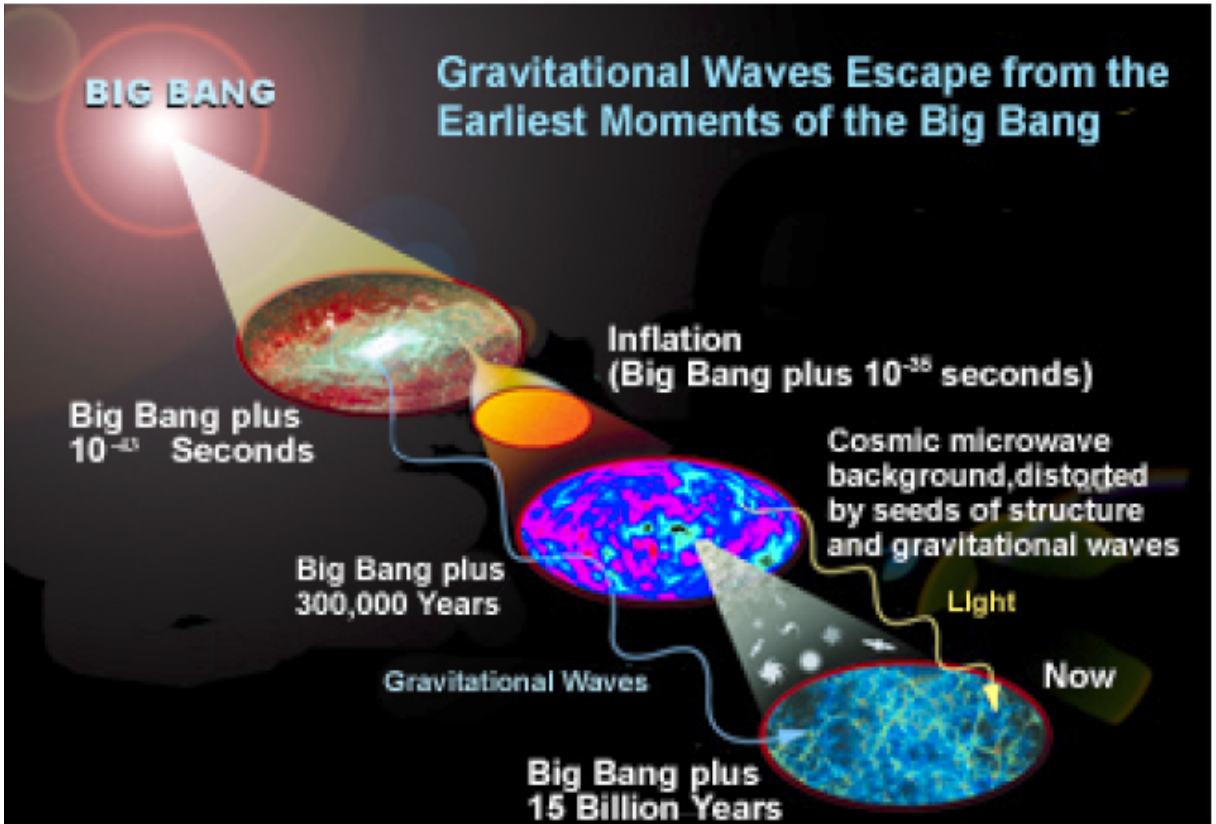

relic gravitational waves signal

- The very early universe
- Phase transitions
  – Bubble collisions
  – Sound waves
- Turbulence
  – Hydro- turbulence
  – MHD turbulence

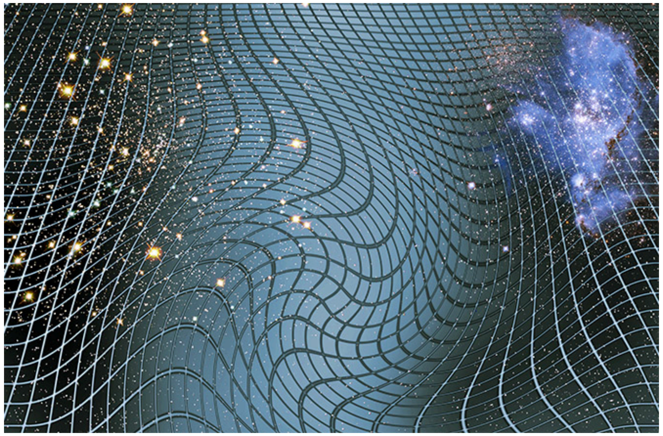

some relations

- To rescale gravitational waves amplitude and frequency:

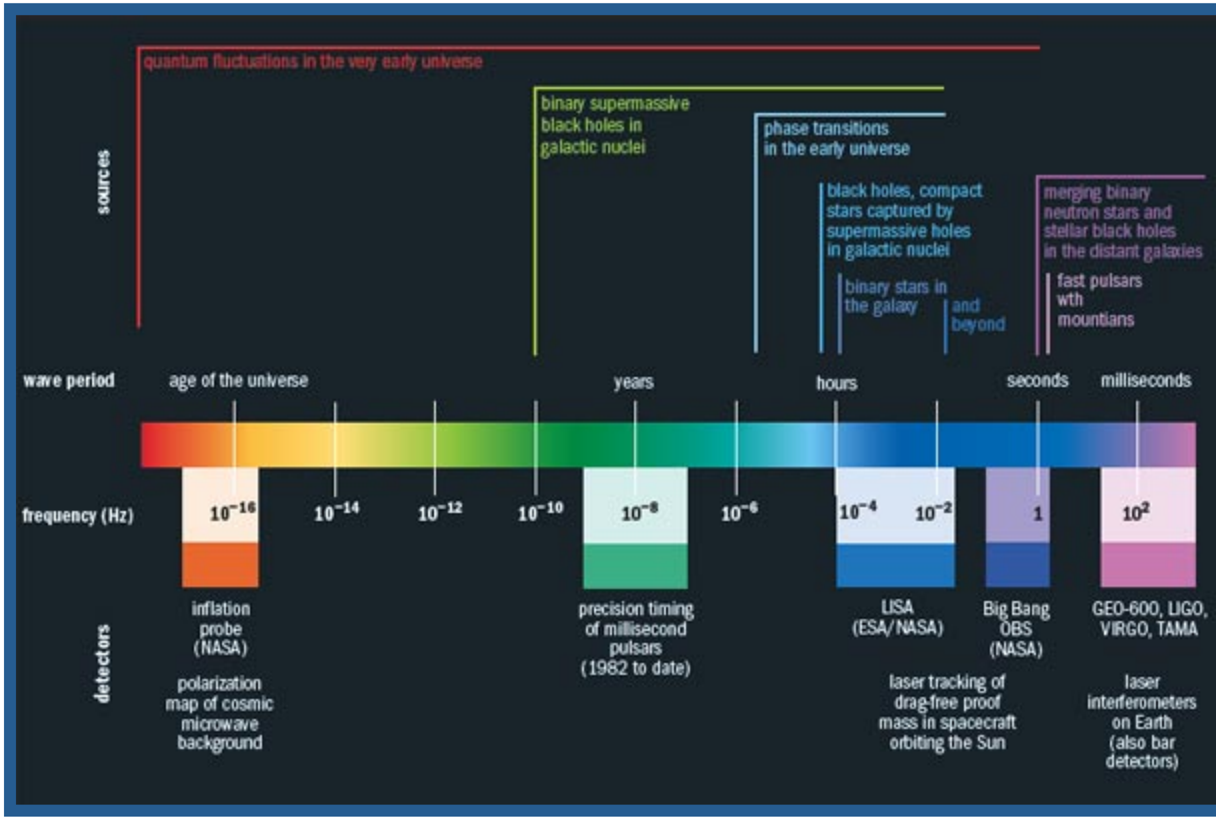

$$\frac{a_\star}{a_0} = 8 \times 10^{-16} \left(\frac{100\mathrm{Gev}}{T_\star}\right) \left(\frac{100}{g_\star}\right)^{\frac{1}{3}},$$

- Hubble frequency measured today:

$$f_{\mathrm{H}} = 1.6 \times 10^{-5}\mathrm{Hz} \left(\frac{T_\star}{100\mathrm{Gev}}\right) \left(\frac{g_\star}{100}\right)^{\frac{1}{6}}$$

gravitational waves polarization

- If the parity in the early universe is violated – relic gravitational waves are polarized.
- The standard model predicts unpolarized gravitational waves

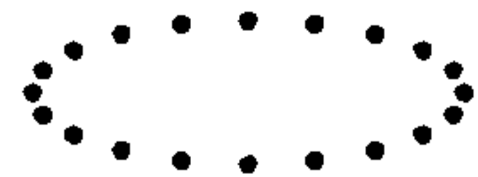

Linearly polarized

Circularly polarized

LISA sensitivity & electroweak scale physics

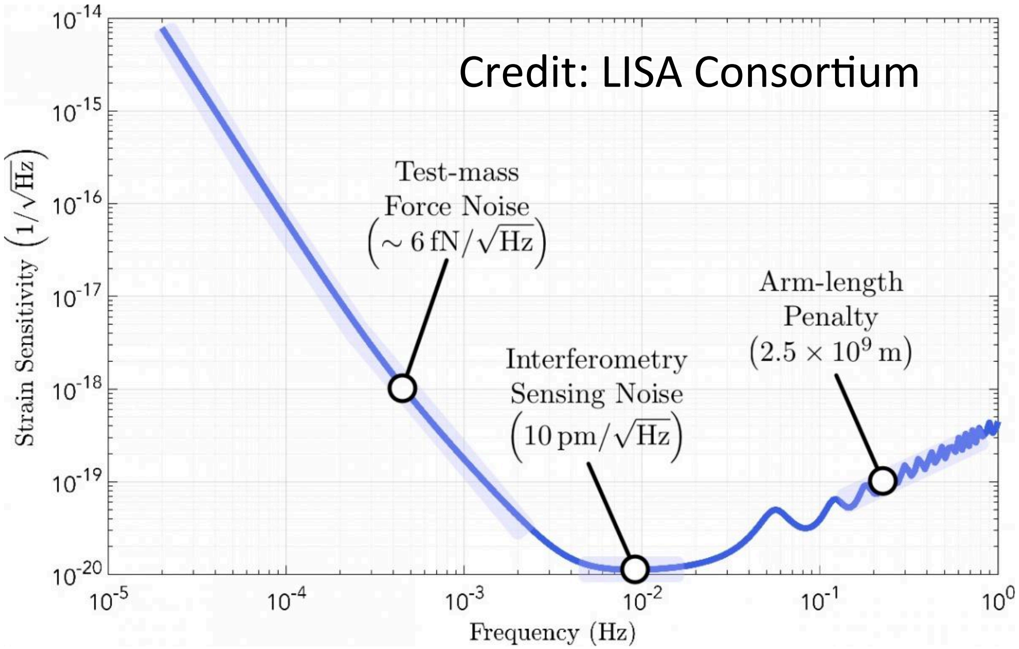

https://www.lisamission.org/multimedia/image/lisa-sensitivity

- **LISA's peak sensitivity corresponds to ~ 1/10 of Hubble horizon at 1 TeV energy scale**
- Hubble frequency $f_0=10^{-4}$Hz (T/1Tev)

Large Hadron Collider (LHC) vs relic gravitational waves: Detecting New Physics?

relic gravitational waves from phase transitions

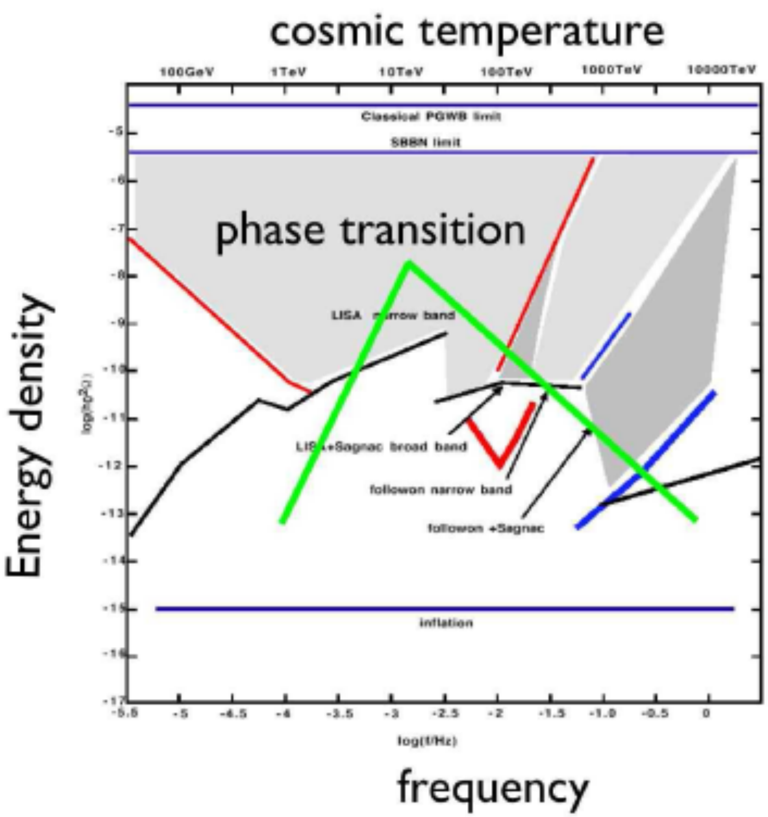

:

C. Hogan, 2006

Pioneering works:

- Winicour 1973
- Hogan 1982, 1986
- Turner & Wilczek 1990
- Kosowsky et al. 1992
- Kosowsky & Turner 1993
- Kamionkowski et al. 1994

physics of phase transitions

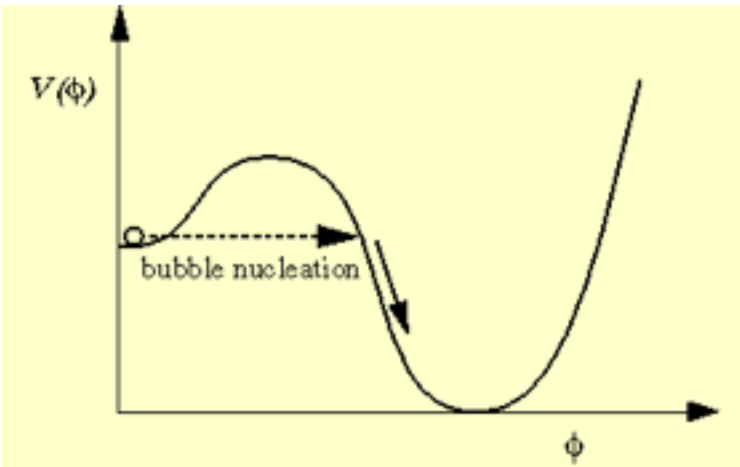

Bubbles of the low-temperature phase are nucleated at random places in the high-temperature phase. The energy difference between the two phases creates an effective outward force on the bubble, causing it to expand and as a result collide with other bubbles.

Bubbles collisions and nucleation

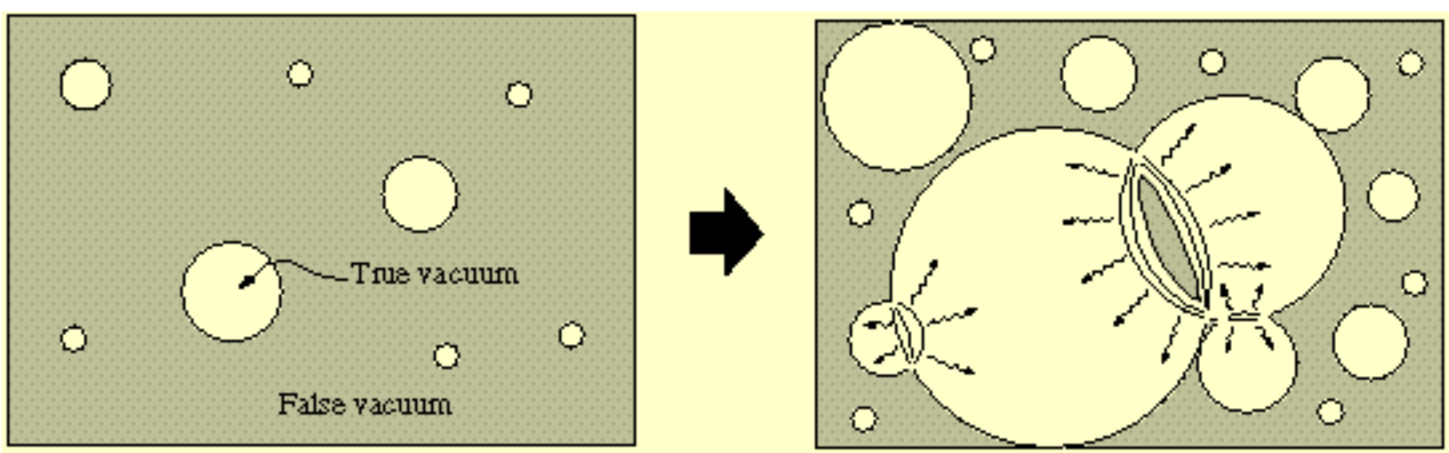

bubbles collisions & sound waves

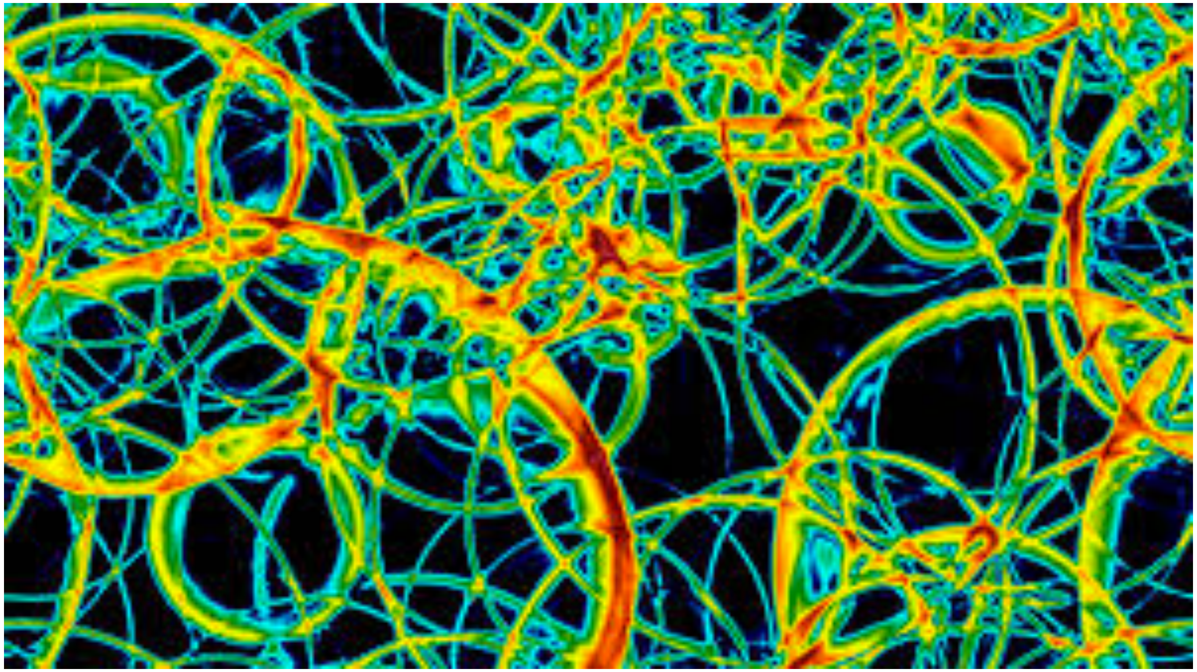

see Mark Hindmarsh and David Weir talks

LISA Cosmology working group logo

primordial turbulence

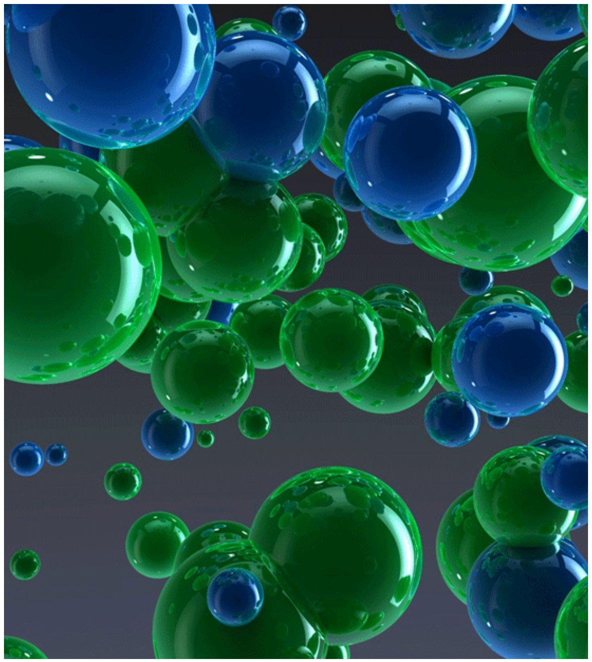

Vacuum bubbles in the early universe
(unlicensed artist's image)

hydro-turbulence vs. gravitational waves

"Van Gogh's Turbulent Mind Captured Turbulence" credit Cosmos and Culture, 2015

- *Kosowsky, Mack, Kahniashvili, 2002*
- *Dolgov, Grasso, Nicolis, 2002*
- *Nicolis, 2004*
- *Kahniashvili, Gogoberidze, Ratra, 2005*

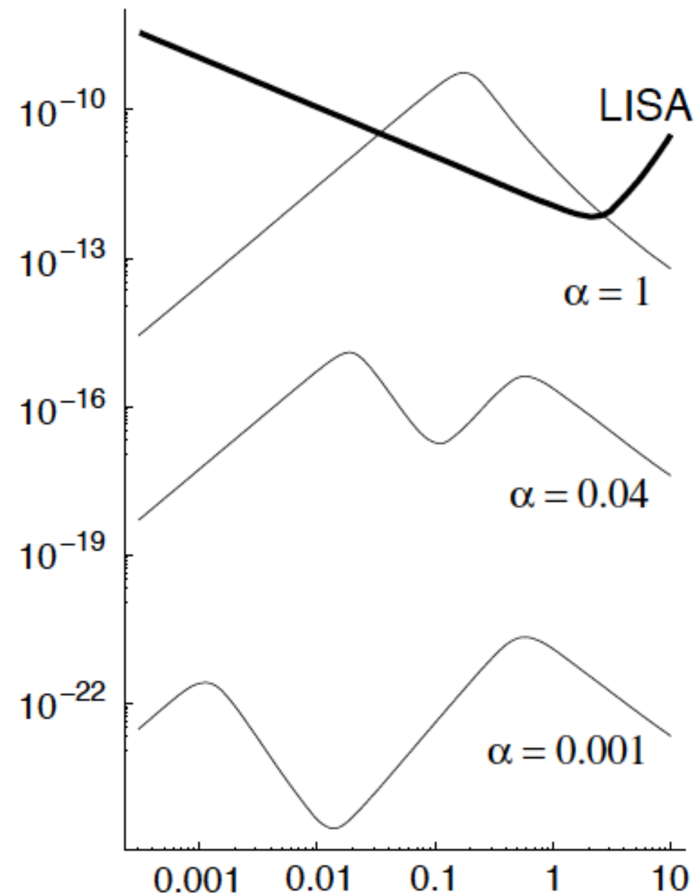

Nicolis 2004

sound waves from turbulence

Aeroacoustic:
Sound waves generation by turbulence

$$\left(\frac{\partial^2}{\partial t^2} - c_{\mathrm{s}}^2\nabla^2\right)\rho' = \frac{\partial^2 T_{ij}}{\partial x_i \partial x_j},$$

Lighthill, 1952
Proudman 1952

aero-acoustic approximation

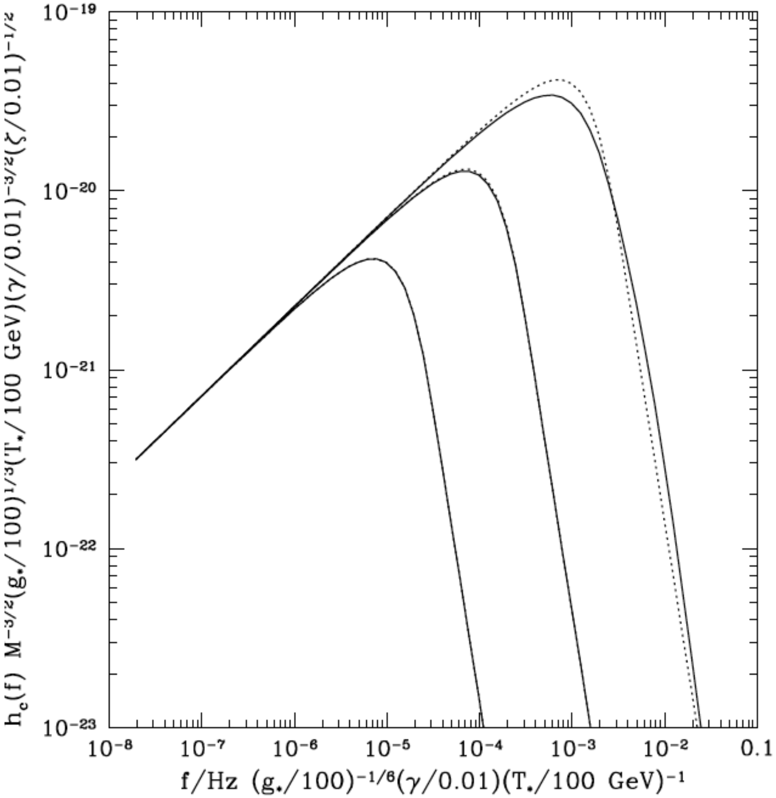

$$\nabla^2 h_{ij}(\mathbf{x},t) - \frac{\partial^2}{\partial t^2} h_{ij}(\mathbf{x},t) = -16\pi G S_{ij}(\mathbf{x},t).$$

Gogoberidze, Kahniashvili, Kosowsky 2007

Parameters:

τ_T turbulence lasting time

k_0 stirring scale

$M = v_0/c$ - Mach number

$R^{3/4}=k_d/k_0$ - Reynolds number

$$\gamma H_*^{-1} = 2\pi/k_0, \qquad \zeta H_*^{-1} = \tau_T;$$

$$f = 1.65\times10^{-3}\,\mathrm{Hz}\left(\frac{\omega_*}{k_0}\right)\left(\frac{g_*}{100}\right)^{1/6}\left(\frac{\gamma}{0.01}\right)^{-1}\left(\frac{T_*}{100\,\mathrm{GeV}}\right),$$

$$h_c(f) = 1.28\times10^{-19}\left(\frac{100\,\mathrm{GeV}}{T_*}\right)\left(\frac{100}{g_*}\right)^{1/3}\left(\frac{\gamma}{0.01}\right)^{3/2}\left(\frac{\zeta}{0.01}\right)^{1/2}\left[k_0^3\omega_*(f)H_{ijij}(\omega_*(f),\omega_*(f))\right]^{1/2}.$$

primordial MHD turbulence

- primordial plasma is perfect conductor
- interaction between primordial magnetic fields and fluid (plasma)
- development of turbulence

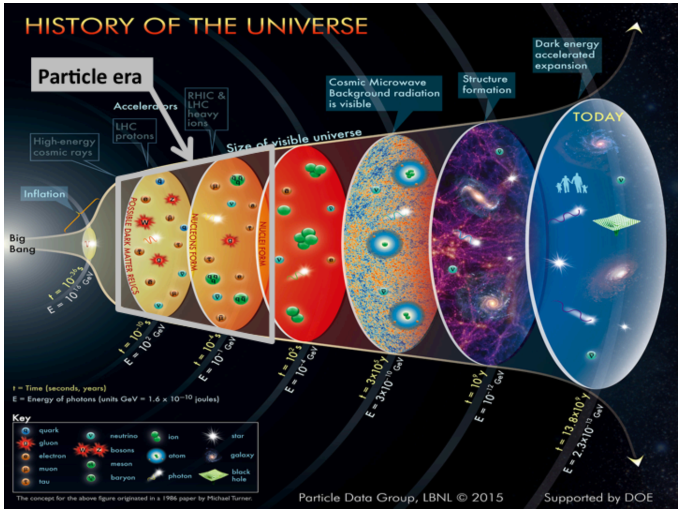

why primordial MHD?

- cosmic magnetic fields
  - astrophysical mechanism
  - cosmological seeds
- observations
  - Fermi data – blazars spectra

PHYSICAL REVIEW VOLUME 75, NUMBER 8 APRIL 15, 1949

On the Origin of the Cosmic Radiation

ENRICO FERMI
Institute for Nuclear Studies, University of Chicago, Chicago, Illinois
(Received January 3, 1949)

A theory of the origin of cosmic radiation is proposed according to which cosmic rays are originated and accelerated primarily in the interstellar space of the galaxy by collisions against moving magnetic fields. One of the features of the theory is that it yields naturally an inverse power law for the spectral distribution of the cosmic rays. The chief difficulty is that it fails to explain in a straightforward way the heavy nuclei observed in the primary radiation.

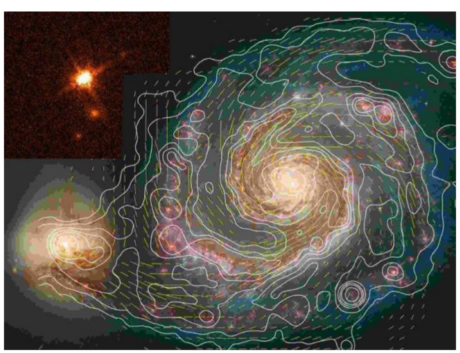

E. Fermi
"On the origin of the cosmic radiation",
PRD, 75, 1169 (1949)

lower limits

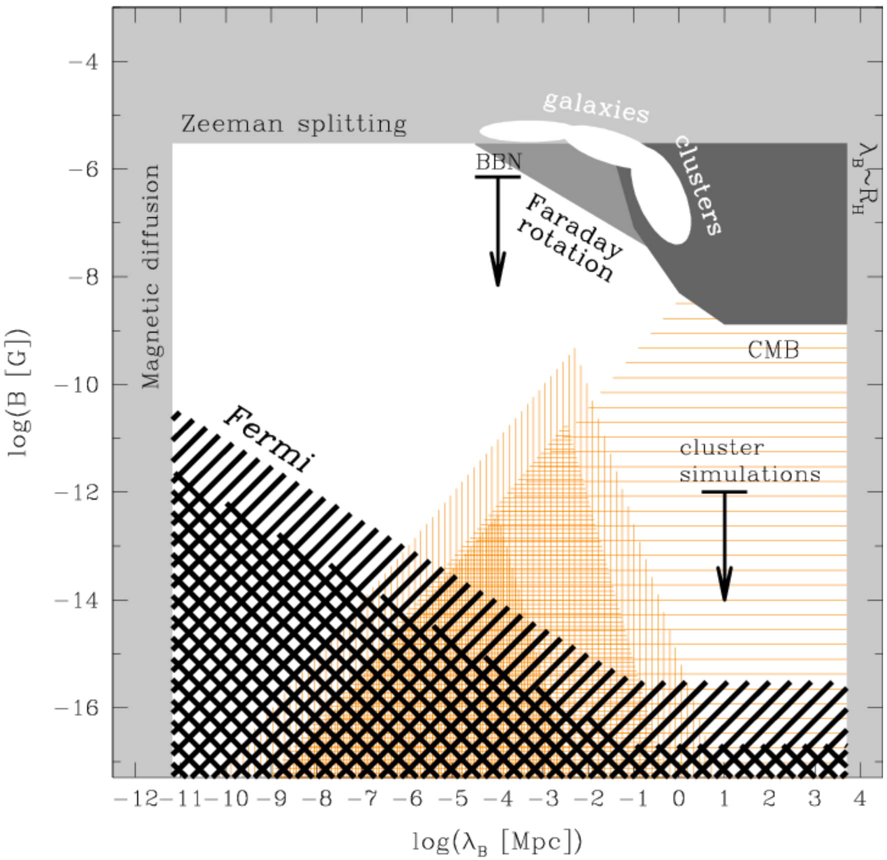

Neronov and Vovk 2010

Time-delay effect: 10^{-18}Gauss

THE ASTROPHYSICAL JOURNAL LETTERS, 733:L21 (5pp), 2011 June 1 doi:10.1088/2041-8205/733/2/L21

TIME DELAY OF CASCADE RADIATION FOR TeV BLAZARS AND THE MEASUREMENT OF THE INTERGALACTIC MAGNETIC FIELD

CHARLES D. DERMER[1], MASSIMO CAVADINI[2], SOEBUR RAZZAQUE[1,6], JUSTIN D. FINKE[1], JAMES CHIANG[3], AND BENOIT LOTT[4,5]
[1] Space Science Division, U.S. Naval Research Laboratory, Washington, DC 20375, USA; charles.dermer@nrl.navy.mil
[2] Dipartimento di Fisica e Matematica, Universitá dell'Insubria, via Valleggio 11, 22100, Como, Italy
[3] W. W. Hansen Experimental Physics Laboratory, Kavli Institute for Particle Astrophysics and Cosmology, Department of Physics and SLAC National Accelerator Laboratory, Stanford University, Stanford, CA 94305, USA
[4] CNRS/IN2P3, Centre d' Études Nucléaires Bordeaux Gradignan, UMR 5797, Gradignan, 33175, France
[5] 40 Université de Bordeaux, Centre d' Études Nucléaires Bordeaux Gradignan, UMR 5797, Gradignan, 33175, France
Received 2010 November 27; accepted 2011 April 7; published 2011 May 6

ABSTRACT

Recent claims that the strength B_{IGMF} of the intergalactic magnetic field (IGMF) is $\gtrsim 10^{-15}$ G are based on upper limits to the expected cascade flux in the GeV band produced by blazar TeV photons absorbed by the extragalactic background light. This limit depends on an assumption that the mean blazar TeV flux remains constant on timescales $\gtrsim 2(B_{\mathrm{IGMF}}/10^{-18}\mathrm{G})^2/(E/10\ \mathrm{GeV})^2$ yr for an IGMF coherence length ≈ 1 Mpc, where E is the measured photon energy. Restricting TeV activity of 1ES 0229+200 to ≈3–4 years during which the source has been observed leads to a more robust lower limit of $B_{\mathrm{IGMF}} \gtrsim 10^{-18}$ G, which can be larger by an order of magnitude if the intrinsic source flux above ≈5–10 TeV from 1ES 0229+200 is strong.

A&A 529, A144 (2011)
DOI: 10.1051/0004-6361/201116441

Astronomy & Astrophysics

Extragalactic magnetic fields constraints from simultaneous GeV–TeV observations of blazars

A. M. Taylor[1], I. Vovk[1], and A. Neronov[1]

[1] ISDC Data Centre for Astrophysics, Ch. d'Ecogia 16, 1290 Versoix, Switzerland
e-mail: Andrew.Taylor@unige.ch

Received 5 January 2011 / Accepted 18 March 2011

ABSTRACT

Context. Attenuation of the TeV γ-ray flux from distant blazars through pair production with extragalactic background light leads to the development of electromagnetic cascades and subsequent, lower energy, GeV secondary γ-ray emission. Due to the deflection of VHE cascade electrons by extragalactic magnetic fields (EGMF), the spectral shape of this arriving cascade γ-ray emission is dependent on the strength of the EGMF. Thus, the spectral shape of the GeV–TeV emission from blazars has the potential to probe the EGMF strength along the line of sight to the object. Constraints on the EGMF previously derived from the gamma-ray data suffer from an uncertainty related to the non-simultaneity of GeV and TeV band observations.
Aims. We investigate constraints on the EGMF derived from observations of blazars for which TeV observations simultaneous with those by *Fermi* telescope were reported. We study the dependence of the EGMF bound on the hidden assumptions it rests upon.
Methods. We select blazar objects for which simultaneous Fermi/LAT GeV and Veritas, MAGIC or HESS TeV emission have been published. We model the development of electromagnetic cascades along the gamma-ray beams from these sources using Monte Carlo simulations, including the calculation of the temporal delay incurred by cascade photons, relative to the light propagation time of direct γ-rays from the source.
Results. Constraints on the EGMF could be derived from the simultaneous GeV–TeV data on the blazars RGB J0710+591, 1ES 0229+200, and 1ES 1218+304. The measured source flux level in the GeV band is lower than the flux of the expected cascade component calculated under the assumption of zero EGMF. Assuming that the reason for the suppression of the cascade component is the extended nature of the cascade emission, we find that $B \gtrsim 10^{-15}$ G (assuming an EGMF correlation length of ≥ 1 Mpc) is consistent with the data. Alternatively, the assumption that the suppression of the cascade emission is caused by the time delay of the cascade photons the data are consistent with $B \gtrsim 10^{-17}$ G for the same correlation length.

Key words. astroparticle physics – magnetic fields – radiative transfer

improved lower limits

$B > 3 \times 10^{-14}$ G ($\lambda_B > 0.03$-0.1 Mpc)

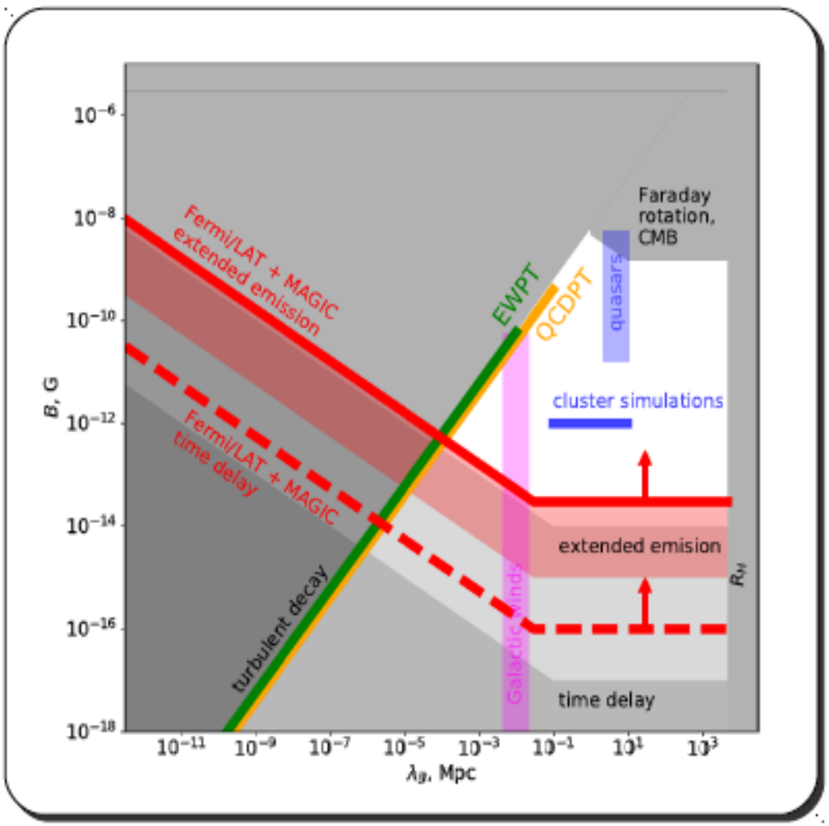

Image by Iugen Vovk

S. Archambault et al. [VERITAS Collaboration],
"Search for Magnetically Broadened Cascade Emission From Blazars with VERITAS," Astrophys. J. 835 , 288 (2017).

M. Ackermann, et al. [Fermi-LAT Collaboration],
"The Search for Spatial Extension in High-latitude Sources Detected by the Fermi Large Area Telescope," Astrophys. J. Suppl. 237 , 32 (2018).

primordial or astrophysical origin?

E ASTROPHYSICAL JOURNAL LETTERS, 727:L4 (4pp), 2011 January 20 doi:10.1088/2041-8205/727/1/L4

LOWER LIMIT ON THE STRENGTH AND FILLING FACTOR OF EXTRAGALACTIC MAGNETIC FIELDS

K. DOLAG[1,2], M. KACHELRIESS[3], S. OSTAPCHENKO[3,4], AND R. TOMÀS[5]
[1] Universitätssternwarte München, München, Germany
[2] Max-Planck-Institut für Astrophysik, Garching, Germany
[3] Institutt for fysikk, NTNU, Trondheim, Norway
[4] D. V. Skobeltsyn Institute of Nuclear Physics, Moscow State University, Moscow, Russia
[5] II. Institut für Theoretische Physik, Universität Hamburg, Germany
Received 2010 September 16; accepted 2010 November 25; published 2010 December 21

ABSTRACT

High-energy photons from blazars can initiate electromagnetic pair cascades interacting with the extragalactic photon background. The charged component of such cascades is deflected and delayed by extragalactic magnetic fields (EGMFs), thereby reducing the observed point-like flux and potentially leading to multi-degree images in the GeV energy range. We calculate the fluence of 1ES 0229+200 as seen by *Fermi*-LAT for different EGMF profiles using a Monte Carlo simulation for the cascade development. The non-observation of 1ES 0229+200 by *Fermi*-LAT suggests that the EGMF fills at least 60% of space with fields stronger than $\mathcal{O}(10^{-16}$ to $10^{-15})$ G for lifetimes of TeV activity of $\mathcal{O}(10^2$ to $10^4)$ yr. Thus, the (non-)observation of GeV extensions around TeV blazars probes the EGMF in voids and puts strong constraints on the origin of EGMFs: either EGMFs were generated in a space filling manner (e.g., primordially) or EGMFs produced locally (e.g., by galaxies) have to be efficiently transported to fill a significant volume fraction as, e.g., by galactic outflows.

4. SUMMARY

We have calculated the fluence of 1ES 0229+200 as seen by *Fermi*-LAT using a Monte Carlo simulation for the cascade development. We have discussed the effect of different EGMF profiles on the resulting suppression of the point-like flux seen by *Fermi*-LAT. Since the electron cooling length is much smaller than the mean free path of the TeV photons, a sufficient suppression of the point-like flux requires that the EGMF fills a large fraction along the line of sight toward 1ES 0229+200, $f \gtrsim 0.6$. The lower limit on the magnetic field strength in this volume is $B \sim \mathcal{O}(10^{-15})$ G, assuming 1ES 0229+200 is stable at least for 10^4 yr, weakening by a factor of 10 for $\tau = 10^2$ yr. These limits put very stringent constraints on the origin of EGMFs. Either the seeds for EGMFs have to be produced by a volume filling process (e.g., primordial) or very efficient transport processes have to be present which redistribute magnetic fields that were generated locally (e.g., in galaxies) into filaments and voids with a significant volume filling factor.

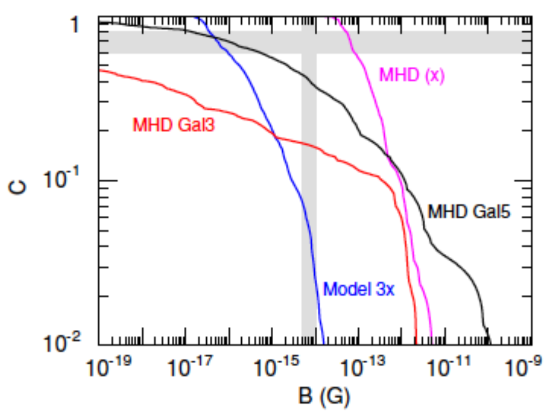

Figure 4. Cumulative volume filling factor $C(B)$ for the four different EGMF models found in MHD simulations.
(A color version of this figure is available in the online journal.)

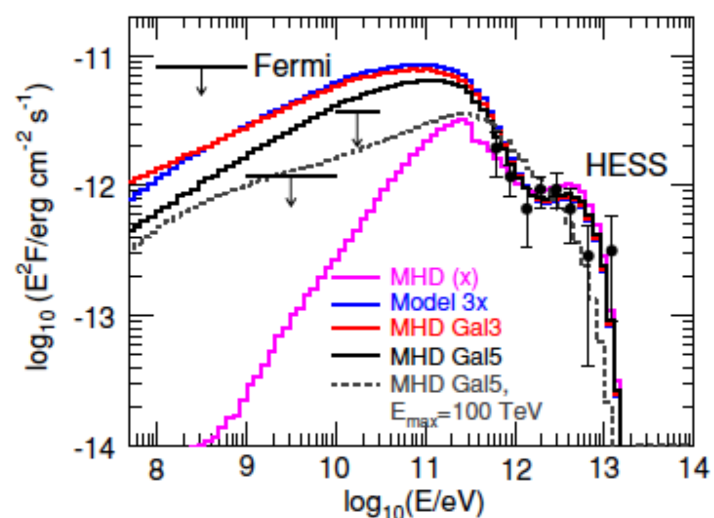

magnetogenesis

F. Hoyle in Proc. ***"La structure et l'evolution de l'Universe"*** **(1958)**

- inflation
- phase transitions
- supersymmetry
- string cosmology
- topological defects

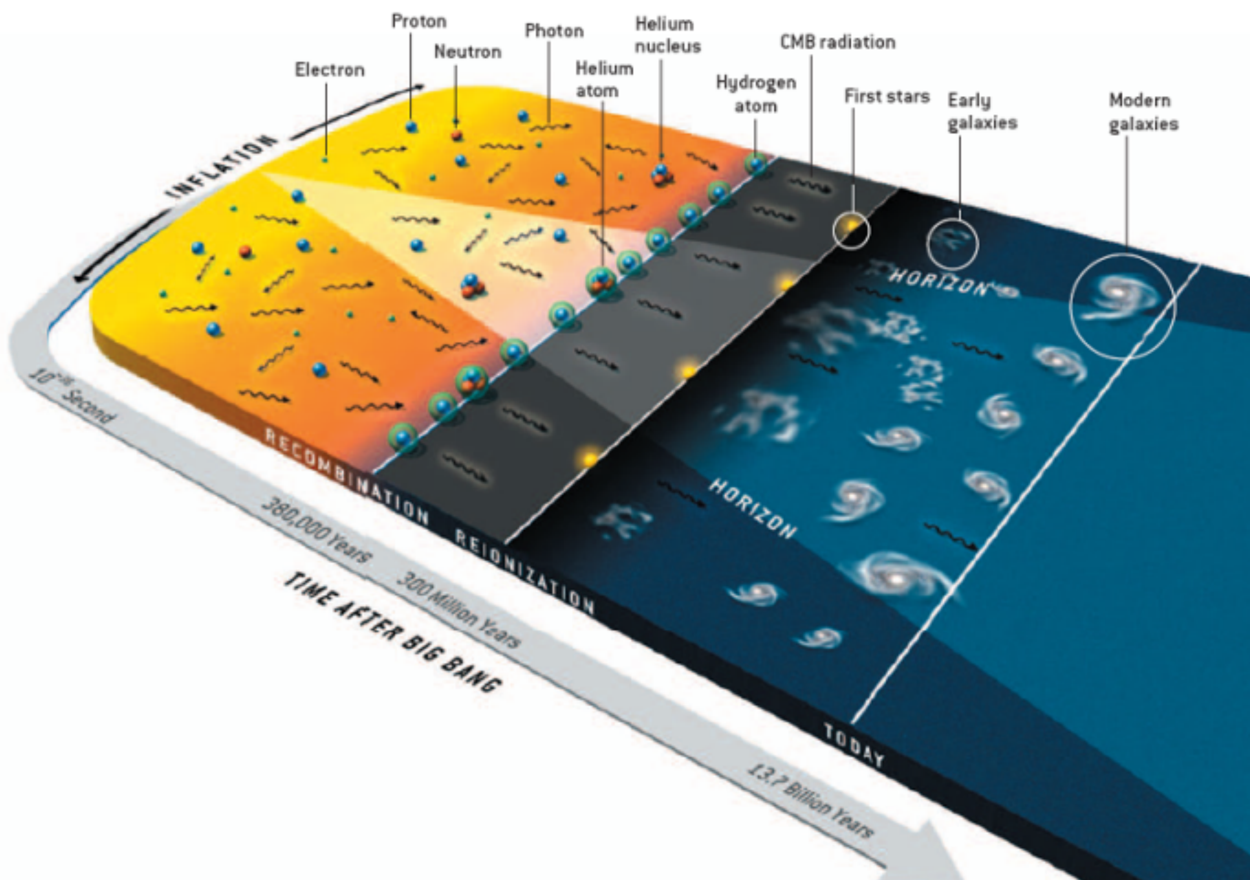

magnetogenesis

- **Inflation**
  - the correlation length larger than horizon
  - scale invariant spectrum
  - well agree with the lower bounds
  - difficulties:
    - backreaction & symmetries violations

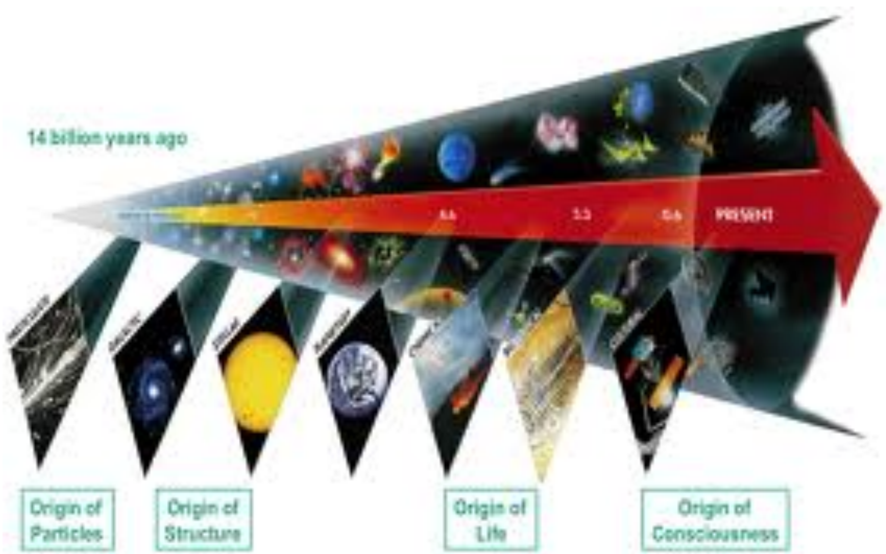

- **Phase transitions**
  - bubble collisions – first order phase transitions QCDPT or EWPT
  - causal fields
  - limited correlation length

- **chiral magnetic effect**

turbulence modeling

- Coupling of the magnetic field with primordial plasma
- Injection of the magnetic energy at a given scale (phase transition bubble)

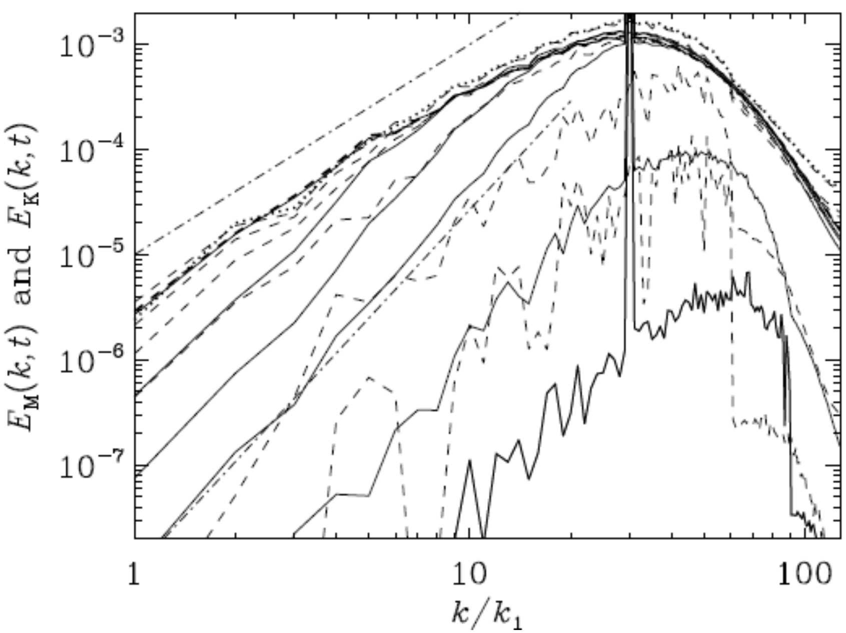

Kahniashvili, Brandenburg, Ratra, Tevzadze 2010

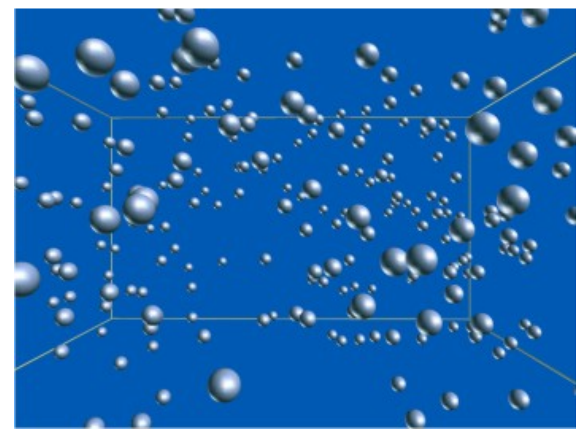

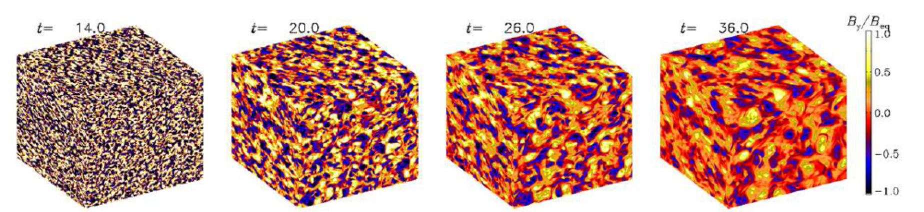

FIG. 2: Evolution of the turbulent magnetic field after turning off the forcing at time $t = 14\,t_1$. The B_y component is shown on the periphery of the computational domain.

MHD turbulence

- Cosmic magnetic field origin – generation in the early universe
- Primordial magnetic fields – effects on phase transition physics
- Generation of turbulence
- MHD turbulence decay

PENCIL CODE 3D compressible MHD

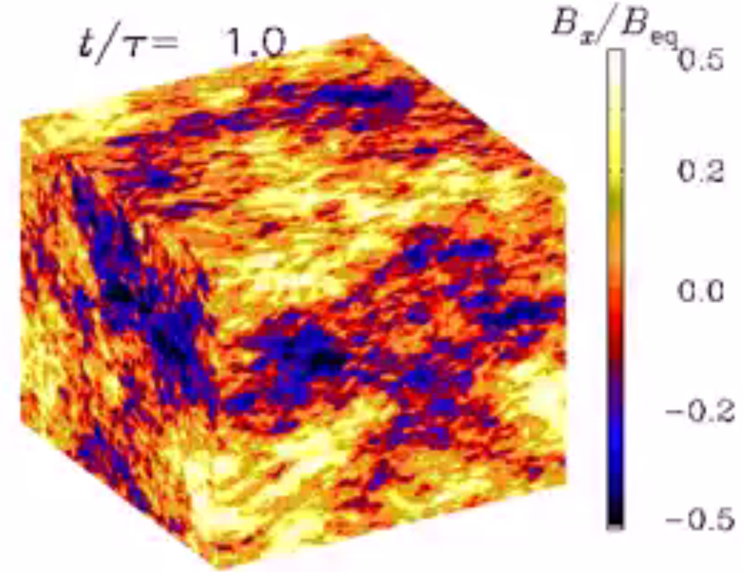

Brandenburg, Kahniashvili, Tevzadze, 2015

there is helicity…

- parity (mirror) symmetry breaking
- matter – antimatter asymmetry
  - baryongenesis
  - leptongenesis
- chiral magnetic effect

$$H_B(t) = \int d^3x \mathbf{A} \cdot \nabla \times \mathbf{A},$$

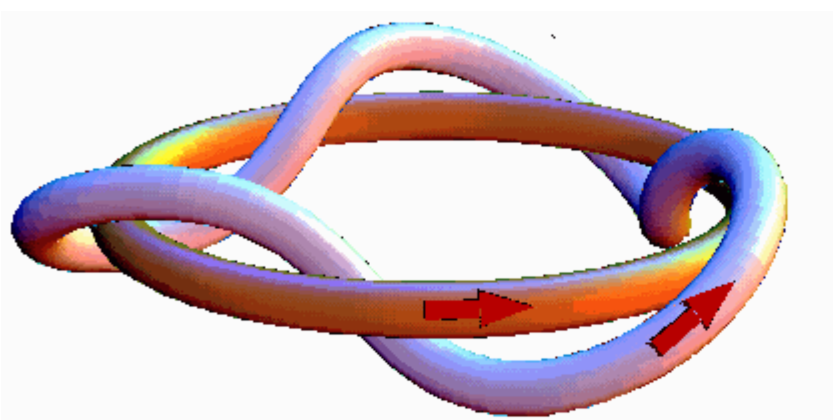

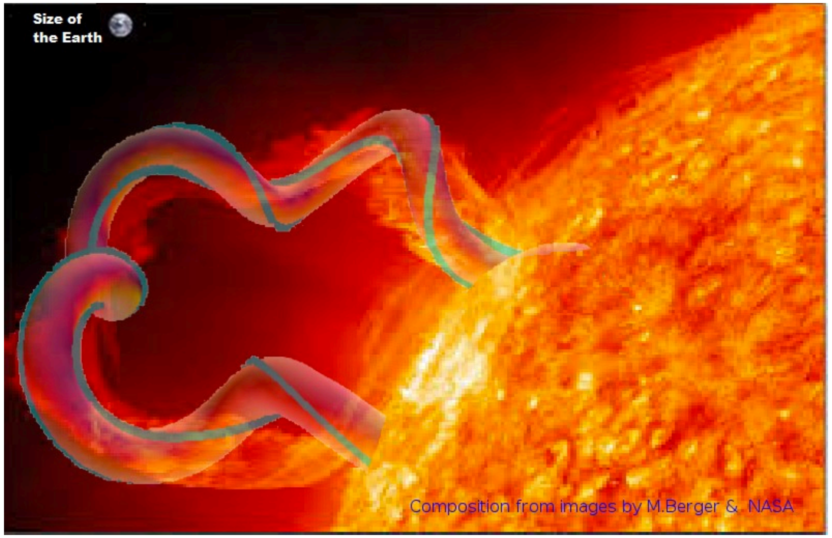

fractional helicity growth

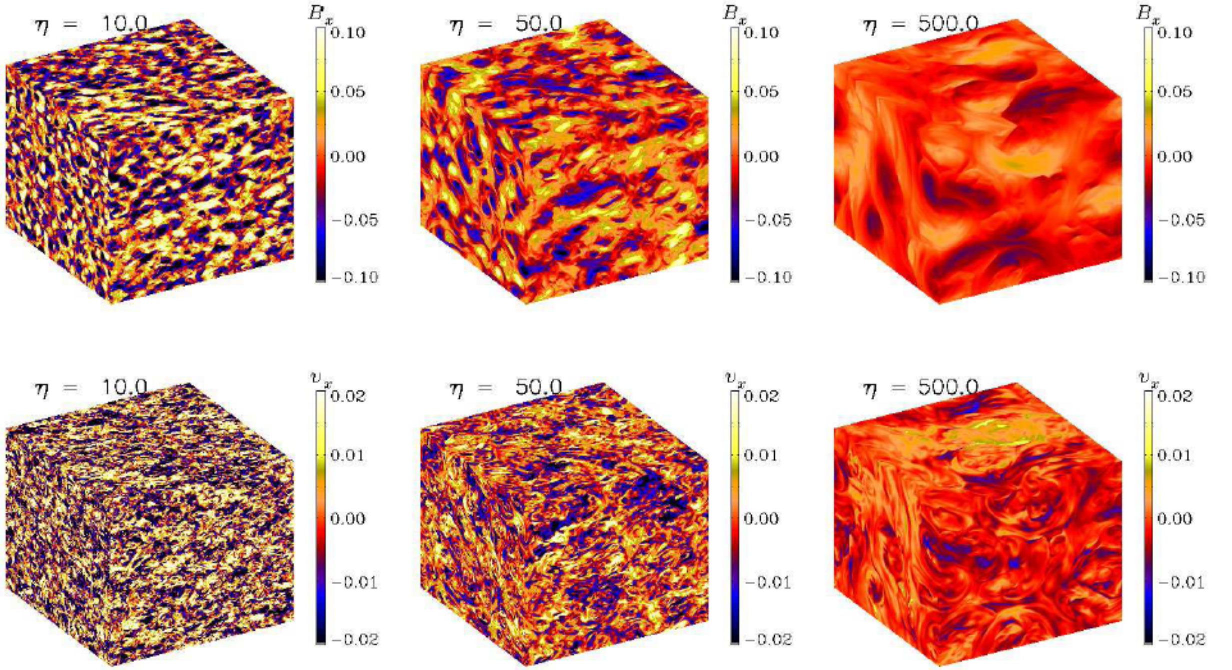

FIG. 2.— Visualizations of B_x (upper row) and v_x (lower row) at three times during the magnetic decay of a weakly helical field with $\sigma = 0.03$.

$$\eta_{\rm fully} = 4\eta_0 \xi_M^2 \mathcal{E}_M^2 / \mathcal{H}_M^2 .$$

Tevzadze et al. 2012

classes of turbulence

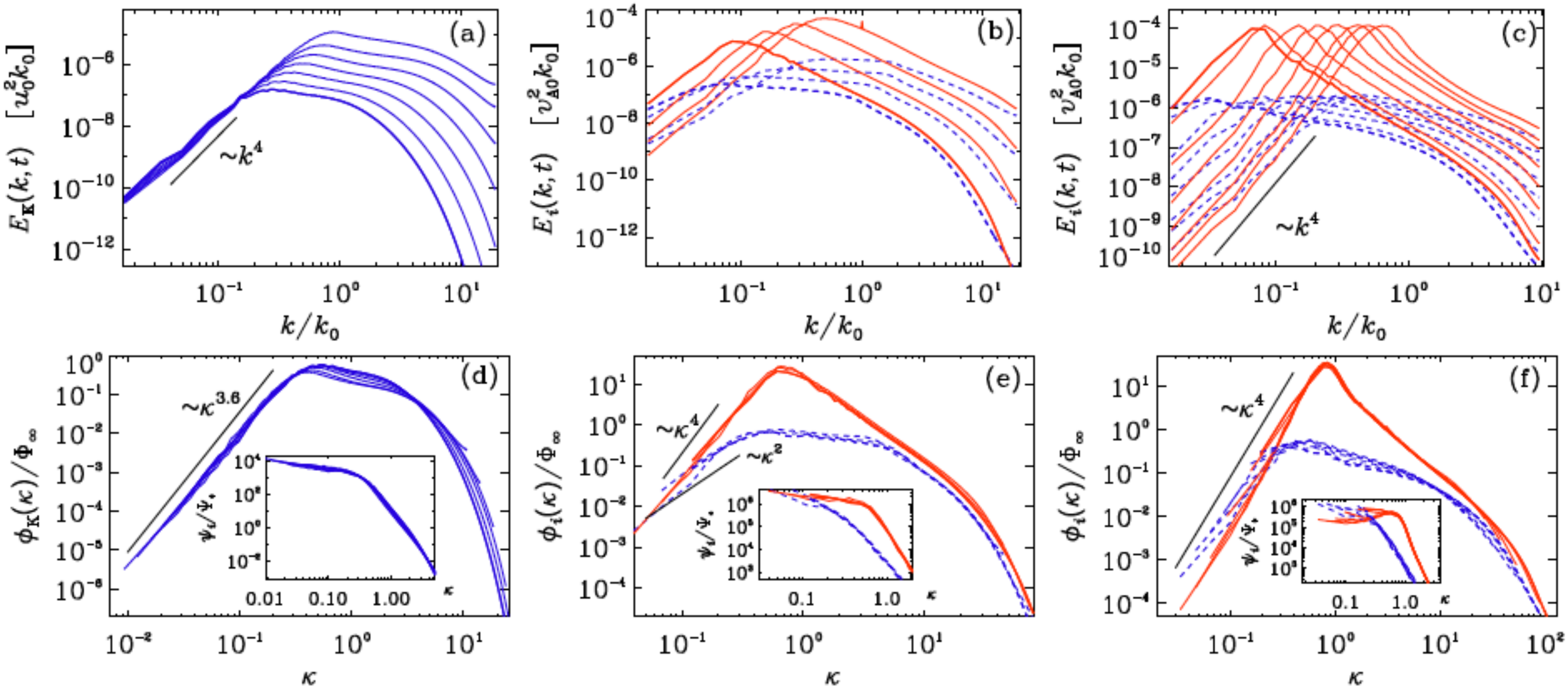

Brandenburg & Kahniashvili 2017

the dynamo effect in decaying helical turbulence

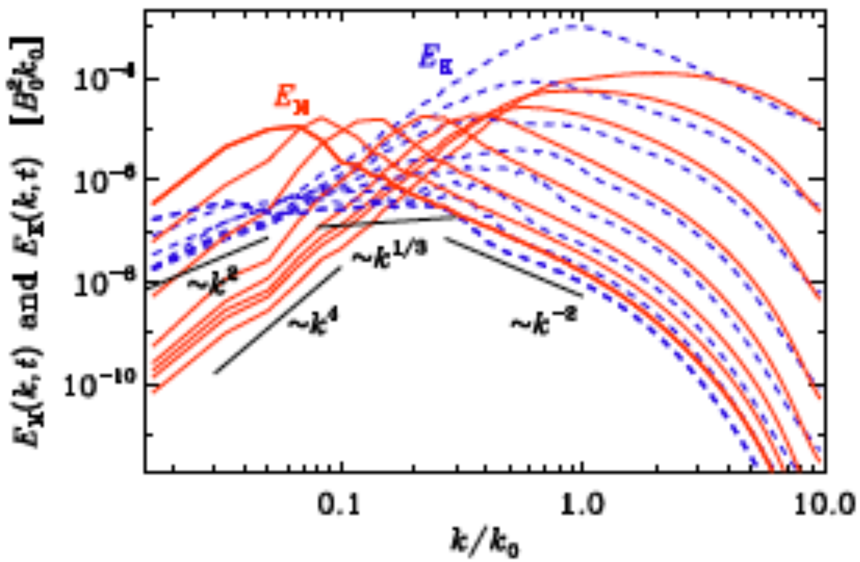

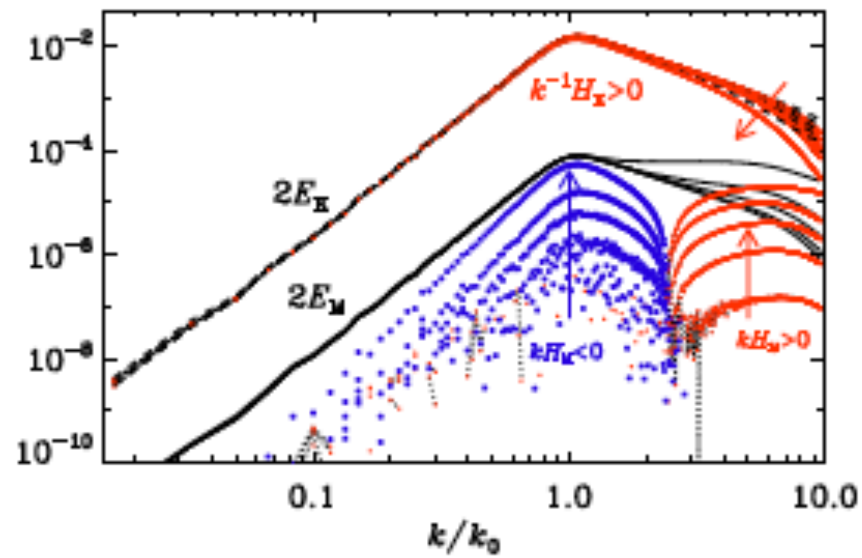

Brandenburg, et al. 2017

chiral MHD turbulence

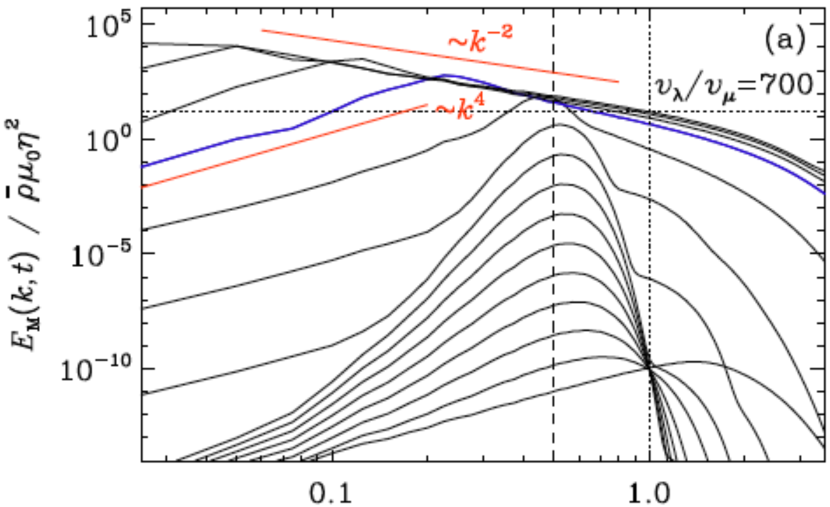

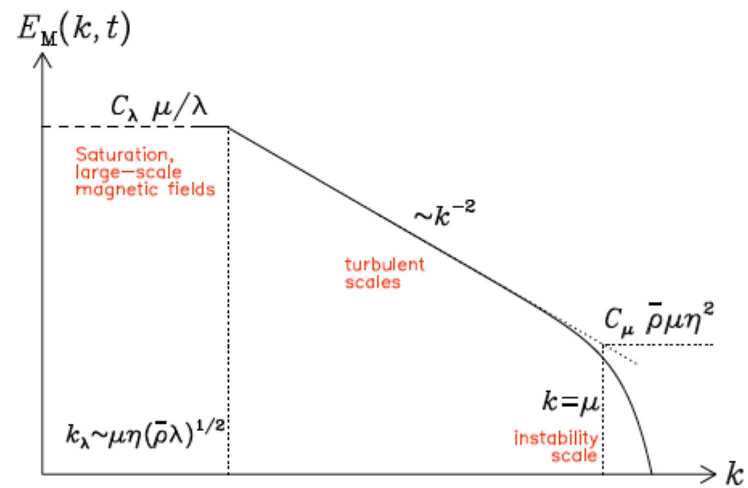

FIG. 1.— Sketch of the magnetic energy spectrum of chiral magnetically driven turbulence.

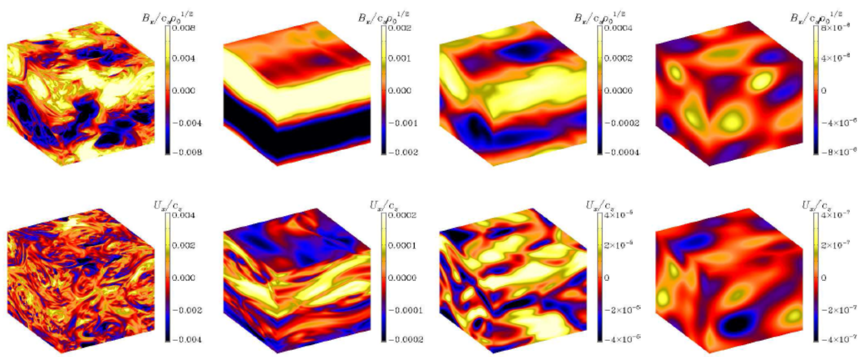

FIG. 3.— B_x and U_x on the periphery of the computational domain for (from left to right) v_λ/v_μ = 700, 70, 7, and 0.07 at the last time.

$$\langle B^2 \rangle \, \xi_M = \epsilon (k_B T_0)^3 (\hbar c)^{-2},$$

Brandenburg et al. 2017

see Igor Rogachevskii talk

Brandenburg, et al. 2017

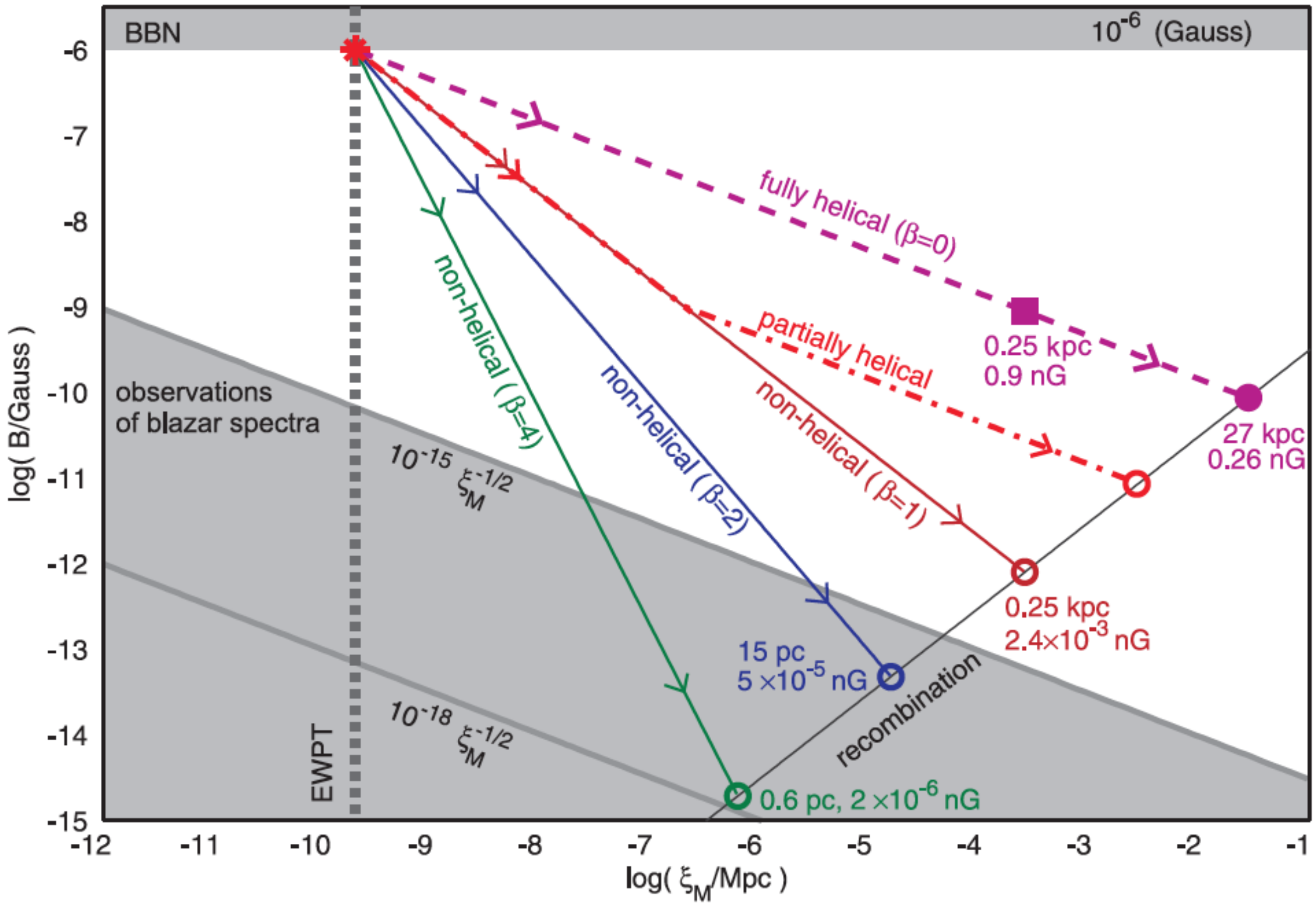

FIG. 11: Turbulent evolution of $B_{\rm rms}$ and $\xi_{\rm M}$ starting from their upper limits given by the BBN bound and the horizon scale at the EWPT for the fully helical case ($B_{\rm rms} \propto \xi_{\rm M}^{-1/2}$), the nonhelical case ($B_{\rm rms} \propto \xi_{\rm M}^{-1}$), and the fractionally helical case with $\epsilon_{{\rm M}\star} = 10^{-3}$. Circles indicate the final points at recombination for zero or partial initial magnetic helicity, the filled circle marks the fully helical case, and the filled square indicates the case with the initial kinetic helicity. The regimes excluded by observations of blazar spectra (upper line: limits claimed by Neronov and Vovk [59], based on the consideration of the expected cascade flux in the GeV band produced by the blazar TeV photons absorbed by the extragalactic background light, and assuming that the mean blazar TeV flux remains constant; bottom line corresponds to the limits obtained through accounting for the fact that the TeV flux activity is limited by the source observation period (few years) [60, 61] and BBN limits are marked in gray. The end of the evolution at recombination is denoted by the straight line given by the relation in Eq. (36), and the final values of $B_{\rm rms}$ and $\xi_{\rm M}$ are indicated for helical and nonhelical scenarios.

inflation generated magnetic fields

Kahniashvili et al. 2012

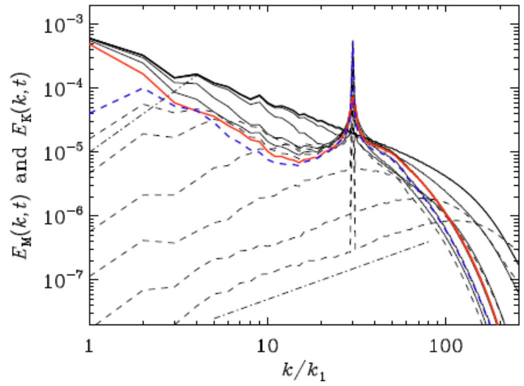

FIG. 2: Magnetic (solid) and kinetic (dashed) energy spectra in regular time intervals. Vortical forcing, $\nu = 10^{-4}$, Pm = 1.

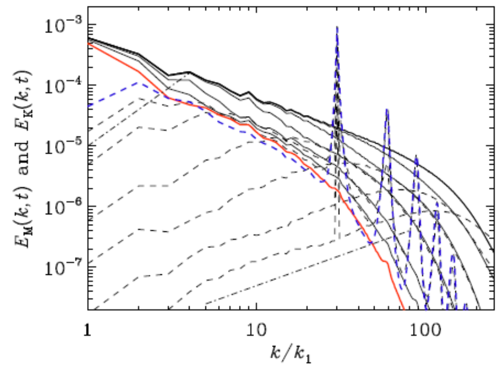

FIG. 4: Potential forcing (plane waves). Run c.

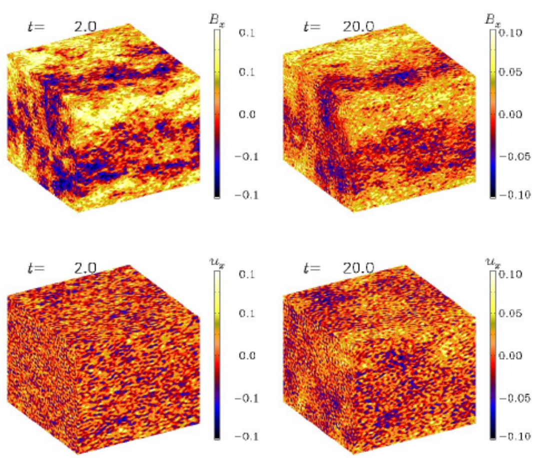

FIG. 6: Visualization of u_x and B_x for the run shown in Fig. 2. (Vortical forcing, $\nu = 10^{-4}$, Pm = 1.)

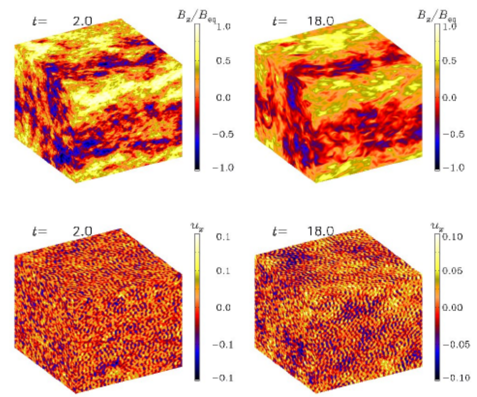

FIG. 8: Visualization of u_x and B_x for the run shown in Fig. 4. Potential forcing (plane waves). Run c.

see Sayan Mandal talk

inflationary magnetogenesis

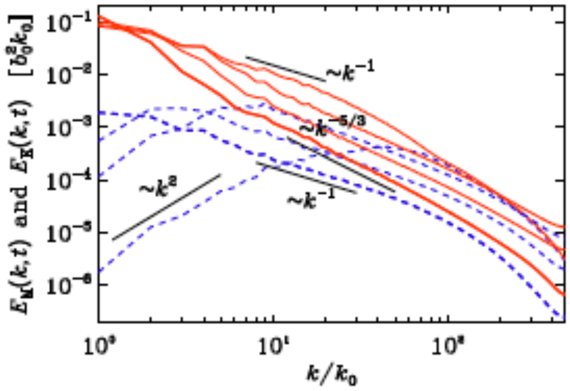

FIG. 2: Magnetic (red solid lines) and kinetic (blue dashed lines) energy spectra for $\sigma = 1$ at times $t/\tau_A = 0.03$, 0.3, 1.2, and 5. The last time is shown in boldface. For orientation, the k^2, k^{-1}, and $k^{-5/3}$ slopes are indicated.

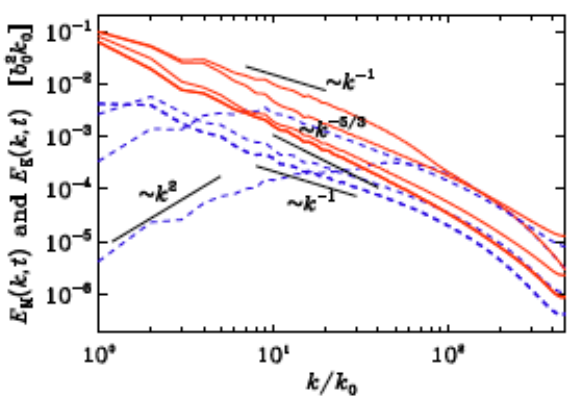

FIG. 3: Same as Fig. 2, but for $\sigma = 0.06$.

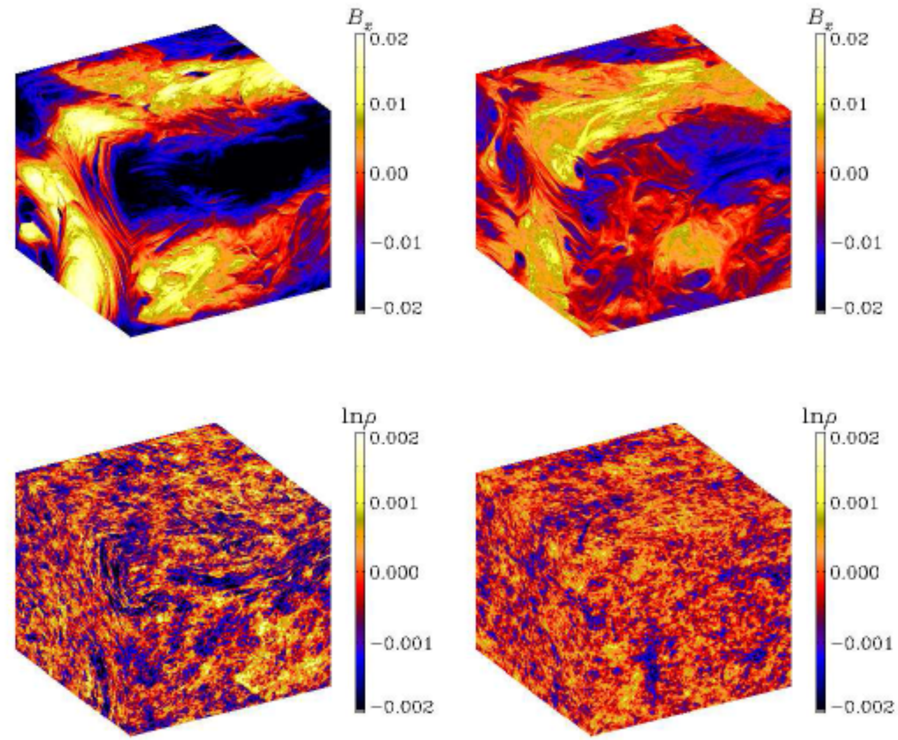

FIG. 7: Comparison of B_z (upper row) and $\ln\rho$ (lower row) for $\sigma = 1$ (left) and $\sigma = 0.06$ (right).

Kahniashvili et al. 2017

see Sayan Mandal talk

importance of MHD

- Cosmic magnetic fields – relic seed magnetic fields
- Effects on turbulence development and generation of sound waves (*Kulsrud 1955*) and gravitational waves
- Enhancement of the signal
  - Wider ranger of frequencies
  - Larger amplitude

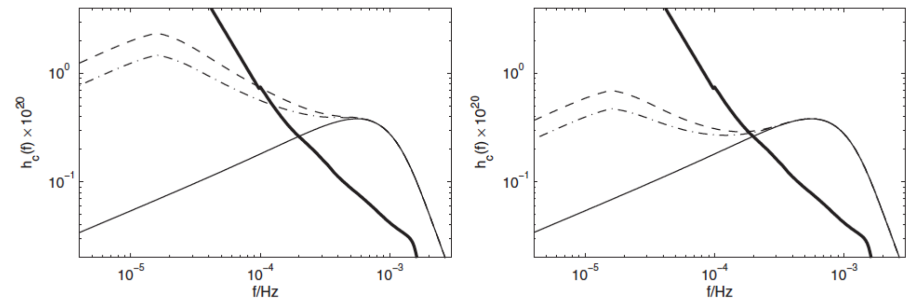

FIG. 1. The spectrum of the gravitational wave strain amplitude, $h_C(f)$, as a function of the frequency f for a first-order phase transition with $g_* = 100$, $T_* = 100$ GeV, $\alpha = 0.5$, and $\beta = 100H_\star$, from hydrodynamic Kolmogorov turbulence with zero magnetic helicity (solid lines) and for the two MHD turbulence models, Model A (dashed-dotted lines) and Model B (dashed lines). The left panel corresponds to initial magnetic helicity $\zeta_\star = 0.15$, while $\zeta_\star = 0.05$ in the right panel. In both panels the bold solid line corresponds to the 1-year, 5σ LISA design sensitivity curve [50] including confusion noise from white dwarf binaries [51].

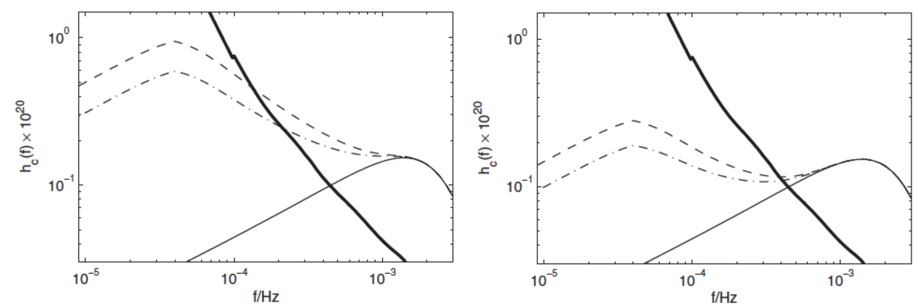

FIG. 2. As in Fig. 1, except now $T_\star = 250$ GeV.

Kahniashvili et al. 2008

phase transitions

- Why MHD is important?
  - wider range of parameters (higher energy scales; supersymmetry)
  - Primordial magnetic field (inflationary?) induced turbulence

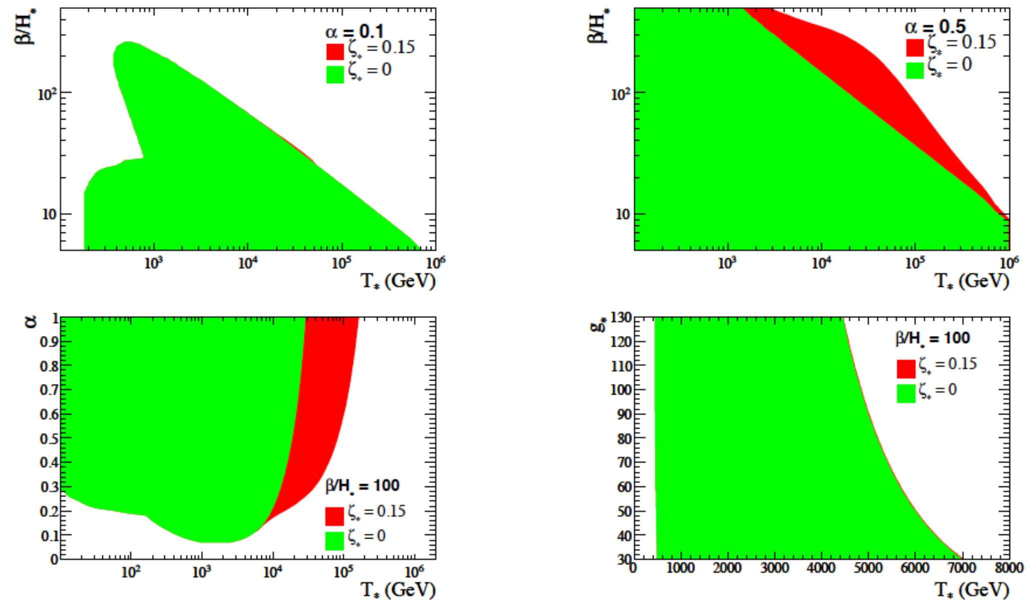

FIG. 3: The LISA sensitivity region in the β/H_* and T_* parameter plane for a phase transition with vacuum energy $\alpha = 0.1$ (left top panel) and $\alpha = 0.5$ (right top panel) [188]. The regions for $\zeta_* = 0$ and $\zeta_* = 0.15$ coincide at these temperatures for $\alpha = 0.1$ (left top panel). The LISA sensitivity region in the α and T_* parameter plane (left bottom panel) with $\beta/H_* = 100$ and $g_* = 100$, and in the g_* and T_* parameter plane (right bottom panel) with $\beta/H_* = 100$ and $\alpha = 0.1$, [188]. A point in parameter space is considered detectable if at any frequency its value of $h_c(f)$ is detectable at a signal-to-noise ratio of 5 in a one-year integration, including the confusion noise from white-draft binaries, based on Refs. [137].

Kahniashvili et al. 2008

numerical simulations

- To account properly non-linear processes (MHD)
- Not be limited by the short duration of the phase transitions
- Two stages turbulence decay
  - Forced turbulence
  - Free decay
- The source is present till recombination (after the field is frozen in)
- Results – strongly initial conditions dependent

see Alberto Roper Pol talk

$$\left(\frac{\partial^2}{\partial t^2} - c^2\nabla^2\right) h_{ij}^{\rm TT} = \frac{16\pi G}{a^3 c^2} T_{ij}^{\rm TT},$$

Grishchuk 1974 $h_{ij}^{\rm TT} = a h_{ij}^{\rm TT,phys}$

$$\mathrm{d}t_{\rm phys} = a\mathrm{d}t$$

The MHD equations for an ultrarelativistic gas in a flat expanding universe [4, 20] are given by

$$\begin{aligned}
\frac{\partial \ln\rho}{\partial t} &= -\frac{4}{3}\left(\boldsymbol{\nabla}\cdot\boldsymbol{u} + \boldsymbol{u}\cdot\boldsymbol{\nabla}\ln\rho\right) \\
&\quad + \frac{1}{\rho c^2}\left[\boldsymbol{u}\cdot(\boldsymbol{J}\times\boldsymbol{B}) + \eta\boldsymbol{J}^2\right], \qquad (4)\\
\frac{\partial \boldsymbol{u}}{\partial t} &= -\boldsymbol{u}\cdot\boldsymbol{\nabla}\boldsymbol{u} + \frac{\boldsymbol{u}}{3}\left(\boldsymbol{\nabla}\cdot\boldsymbol{u} + \boldsymbol{u}\cdot\boldsymbol{\nabla}\ln\rho\right) \\
&\quad - \frac{\boldsymbol{u}}{\rho c^2}\left[\boldsymbol{u}\cdot(\boldsymbol{J}\times\boldsymbol{B}) + \eta\boldsymbol{J}^2\right] - \frac{c^2}{4}\boldsymbol{\nabla}\ln\rho \\
&\quad + \frac{3}{4\rho}\boldsymbol{J}\times\boldsymbol{B} + \frac{2}{\rho}\boldsymbol{\nabla}\cdot(\rho\nu\mathsf{S}) + \boldsymbol{\mathcal{F}}, \qquad (5)\\
\frac{\partial \boldsymbol{B}}{\partial t} &= \nabla\times(\boldsymbol{u}\times\boldsymbol{B} - \eta\boldsymbol{J} + \boldsymbol{\mathcal{E}}), \qquad (6)
\end{aligned}$$

gravitational Waves from turbulence

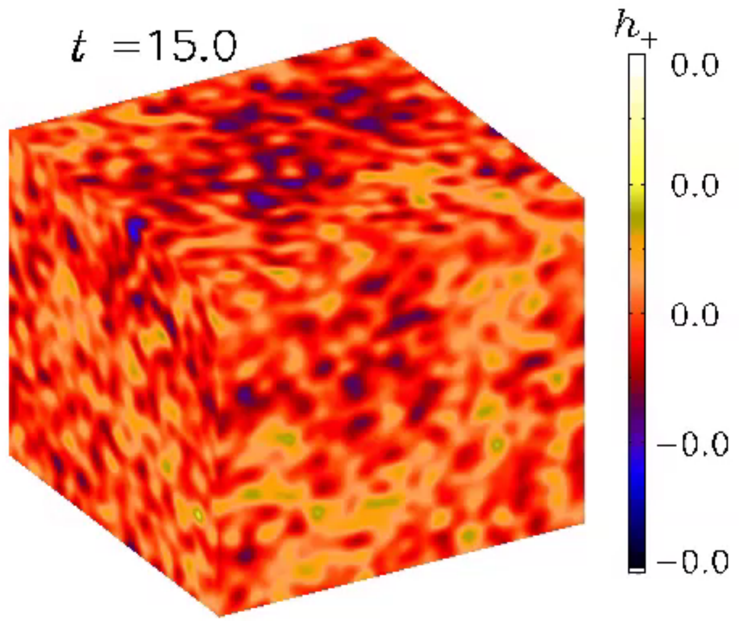

Acoustic turbulence

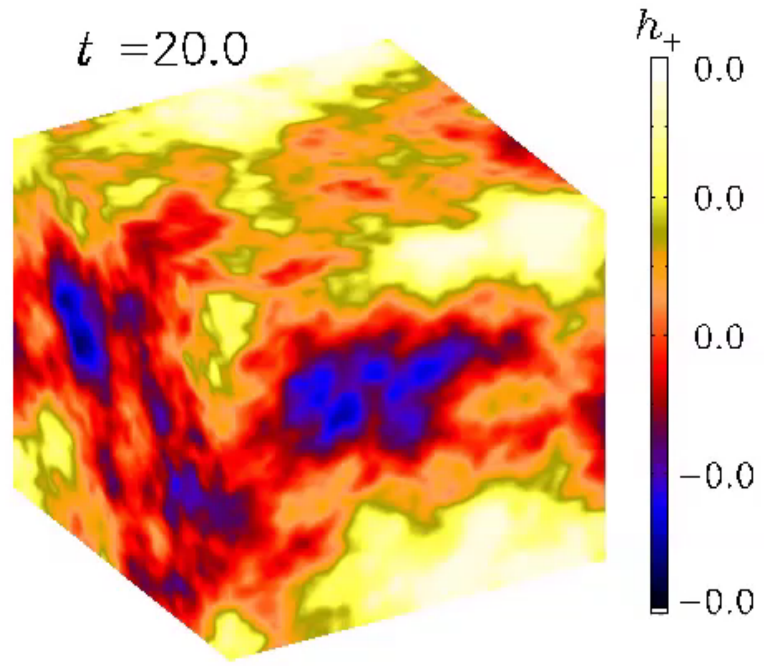

Vortical turbulence

see Axel Brandenburg talk

gravitational waves: results

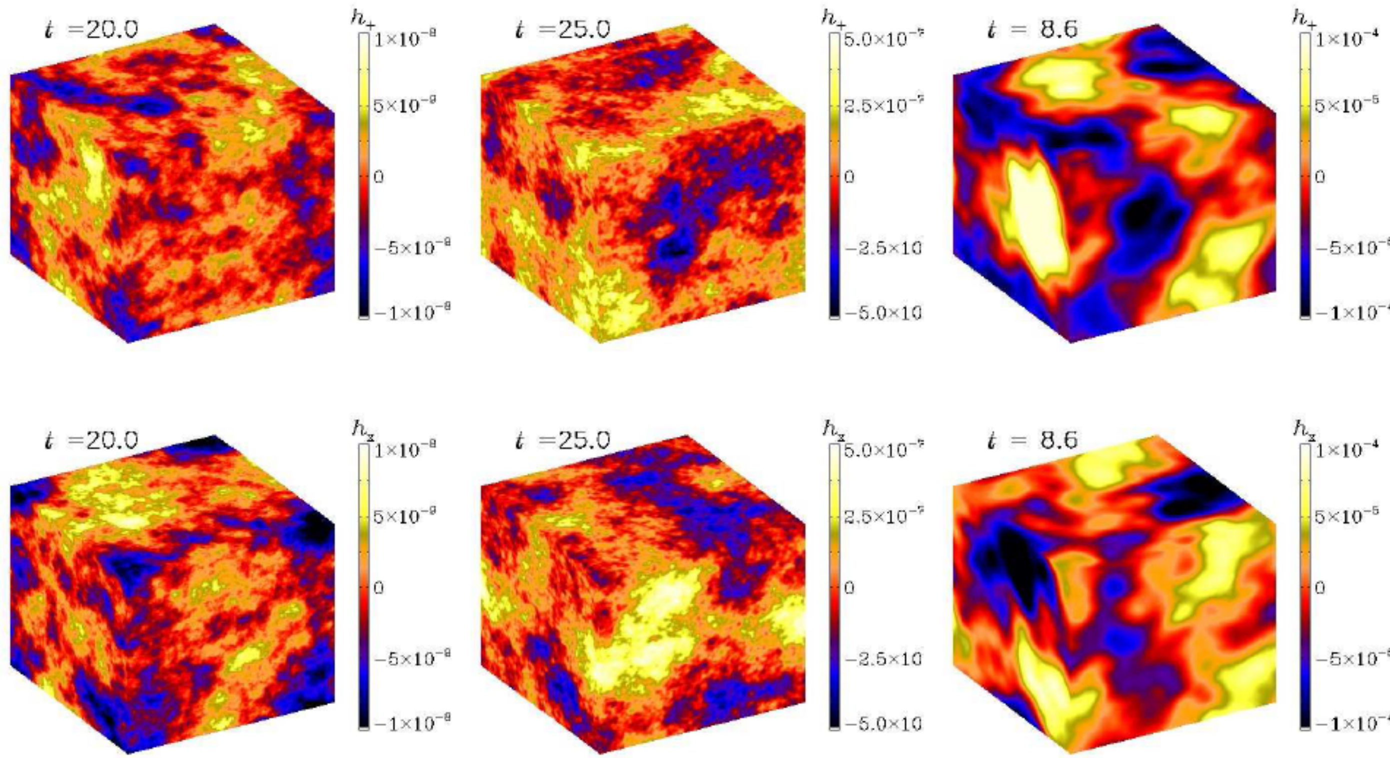

Roper Pol et al. 2019 PRL submitted

$$\tilde{h}_+(\boldsymbol{k},t) = \tfrac{1}{2} e_{ij}^{+}(\boldsymbol{k})\, \tilde{h}_{ij}(\boldsymbol{k},t),$$
$$\tilde{h}_\times(\boldsymbol{k},t) = \tfrac{1}{2} e_{ij}^{\times}(\boldsymbol{k})\, \tilde{h}_{ij}(\boldsymbol{k},t).$$

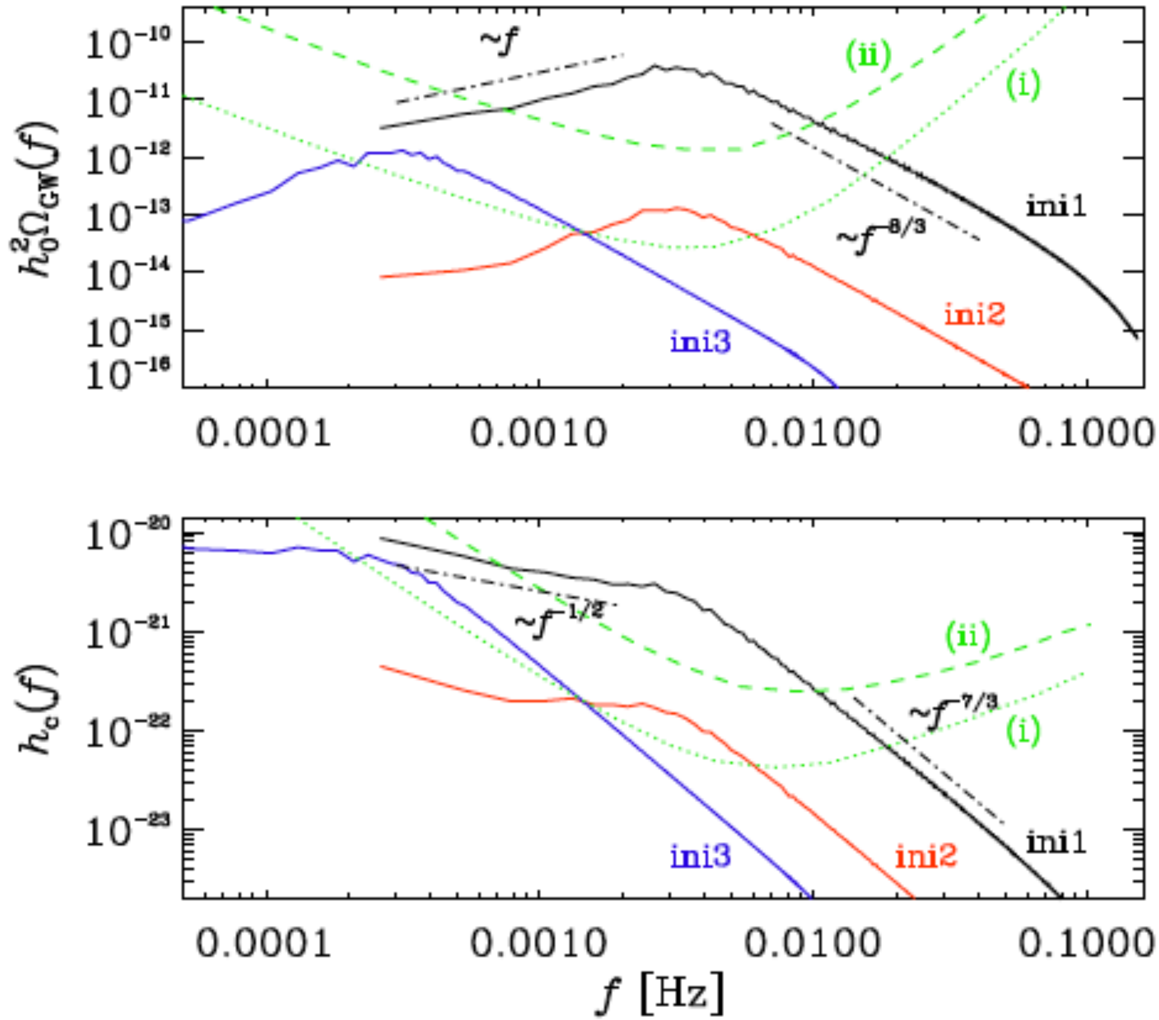

FIG. 2: Spectra of $h_0^2\Omega_{\rm GW}(f)$ and $h_c(f)$ along with the LISA sensitivity curves in (i) the 6-link configurations with 5×10^9 m arm length and (ii) the 4-link configurations with 2×10^9 m arm length after 5 years duration [30, 31]. The dash-dotted lines indicate the slopes 1 and $-8/3$ in the upper panel and $-1/2$ and $-7/3$ in the lower.

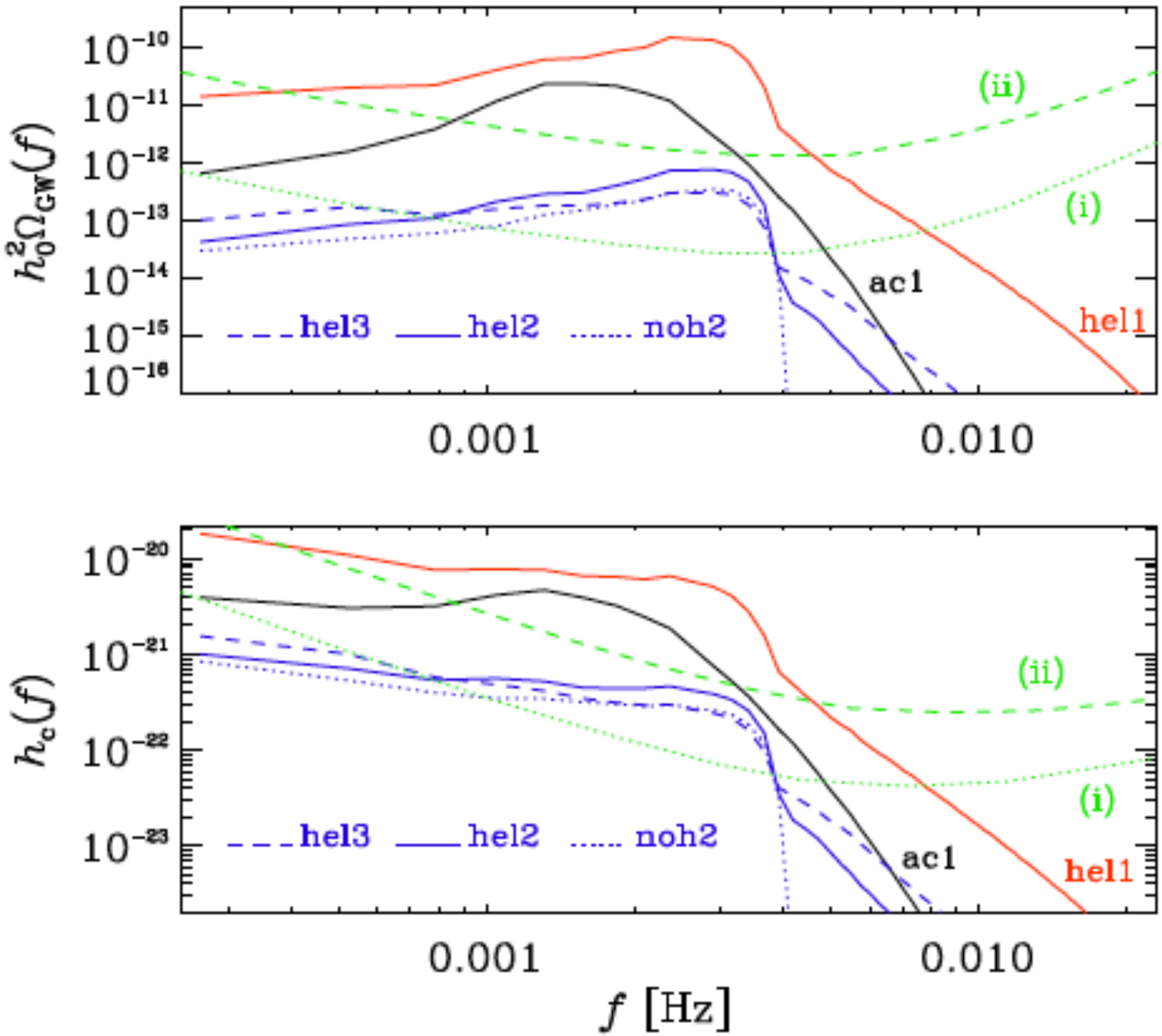

FIG. 4: Similar to Fig. 2, but for Runs hel1–3, noh2, and ac1.

conclusions

- Primordial turbulence is potentially detectable by LISA
- Primordial magnetic fields can serve as seeds for the observed cosmic magnetic fields.
- Presence of primordial magnetic field makes the signal substantially stronger and allows it to spread over a wide range of frequencies.
- LISA mission offers a possibility to understand the physics of phase transitions (and possibly baryogenesis)
- Parity violating sources produce circularly polarized gravitational waves, and the polarization degree might be around 100% (for fully helical sources).

Thank you!

acknowledgement

NORDITA

საქართველოს განათლების,
მეცნიერების, კულტურისა
და სპორტის სამინისტრო

NSF